Dissertation presented to the Instituto Tecnológico de Aeronáutica, in partial fulfillment of the requirements for the Degree of Master in Science in the Program of Aeronautical and Mechanical Engineering, Field of Aerospace Systems and Mechatronics.

Pedro Filizola Sousa Maia Gonçalves

ATTITUDE DETERMINATION OF A MULTIROTOR AERIAL VEHICLE USING CAMERA VECTOR MEASUREMENTS AND GYROS

Dissertation approved in its final version by signatories below:

Prof. Dr. Davi Antônio dos Santos

Advisor

Prof. Dr. Luiz Carlos Sandoval Góes

Prorector of Graduate Studies and Research

Campo Montenegro

São José dos Campos, SP - Brazil

2014

Cataloging-in Publication Data

Documentation and Information Division

Gonçalves, Pedro Filizola Sousa Maia

Attitude Determination of a Multirotor Aerial Vehicle Using Camera Vector Measurements and Gyros / Pedro Filizola Sousa Maia Gonçalves.

São José dos Campos, 2014.

69f.

Dissertation of Master in Science – Course of Aeronautical and Mechanical Engineering. Area of Aerospace Systems and Mechatronics – Instituto Tecnológico de Aeronáutica, 2014. Advisor: Prof. Dr. Davi Antônio dos Santos.

1. Aerial Robotics. 2. Kalman Filter. 3. Attitude Determination. 4. Computer Vision. I. Instituto Tecnológico de Aeronáutica. II. Title.

BIBLIOGRAPHIC REFERENCE

GONÇALVES, Pedro Filizola Sousa Maia. **Attitude Determination of a Multirotor Aerial Vehicle Using Camera Vector Measurements and Gyros**. 2014. 69f. Dissertation of Master in Science in Aerospace Systems and Mechatronics – Instituto Tecnológico de Aeronáutica, São José dos Campos.

CESSION OF RIGHTS

AUTHOR NAME: Pedro Filizola Sousa Maia Gonçalves

PUBLICATION TITLE: Attitude Determination of a Multirotor Aerial Vehicle Using Camera Vector Measurements and Gyros.

PUBLICATION KIND/YEAR: Dissertation / 2014

It is granted to Instituto Tecnológico de Aeronáutica permission to reproduce copies of this dissertation to only loan or sell copies for academic and scientific purposes. The author reserves other publication rights and no part of this dissertation can be reproduced without his authorization.

Pedro Filizola Sousa Maia Gonçalves

Praça Marechal Eduardo Gomes, 50 - Vila das Acácias

CEP 12.228-900 – São José dos Campos-SP

ATTITUDE DETERMINATION OF A MULTIROTOR AERIAL VEHICLE USING CAMERA VECTOR MEASUREMENTS AND GYROS

Pedro Filizola Sousa Maia Gonçalves

Dissertation Committee Composition:

Prof^{a}. Dr^{a}.	Neusa Maria Franco de Oliveira	Chairperson	-	ITA
Prof. Dr.	Davi Antônio dos Santos	Advisor	-	ITA
Prof. Dr.	Hélio Koiti Kuga	External Member	-	INPE
Prof. Dr.	Cairo Lúcio Nascimento Júnior	Member	-	ITA

ITA

To Ana Luiza, my sister, and to Thamires, my wife, I dedicate this work.

Acknowledgments

Thanks to God, for the health and for the capacity to execute this work.

Thanks to my wife, Thamires, for the comprehension and for joining me in this trajectory of our lives.

Thanks to my parents Vicente and Regina, for tolerating the distance and for encouraging my decisions.

Thanks to Professor Davi Santos, for the opportunity and for assisting me to achieve many competences beyond this research.

Thanks to my old friends, and coworkers, Igor Prado and Davi Castro, for the fellowship during this course.

Thanks to Fundação de Amparo à Pesquisa do Amazonas for the grants and to Instituto Tecnológico de Aeronáutica for providing me the structure to conclude this work.

"A multitude of words is no proof of a prudent mind."
Thales of Miletus

Resumo

A utilização de câmeras embarcadas para guiamento e navegação de Veículos Aéreos Não Tripulados (VANTs) tem atraído o foco de muitas pesquisas acadêmicas. Em particular, nos VANTs do tipo multirotor, a câmera é amplamente empregada em aplicações realizadas em ambientes internos, onde há menos acesso ao sinal GNSS e maior interferência eletromagnética. No entanto, tais pesquisas usualmente adotam as imagens obtidas pela câmera para auxiliar à estimação de posição/velocidade linear, mas não especificamente para assistir à determinação de atitude. Esta dissertação propõe um método de determinação de atitude para VANTs do tipo multirotor utilizando pares de medidas vetoriais obtidas a partir de uma câmera fixa ao corpo e apontada para baixo junto com medidas de velocidade angular obtidas por girômetros. O método é constituído de três módulos. O primeiro detecta e identifica marcas no solo utilizando as imagens capturadas. O segundo módulo calcula as medidas vetoriais correspondentes às direções das marcas em relação à câmera. O terceiro módulo é responsável pela estimação da atitude a partir das medidas vetoriais calculadas. O método de estimação empregado consiste numa versão com atualização sequencial do filtro de Kalman Estendido Multiplicativo (MEKF). O método proposto foi avaliado por simulações de Monte Carlo utilizando Simulink 3D Animation. Durante a avaliação, o método se mostrou efetivo e com resultados satisfatórios na maioria dos casos simulados. Finalmente, são sugeridos trabalhos futuros para a potencial continuação da pesquisa.

Palavras–Chave: Robótica Aérea, Filtro de Kalman, Determinação de Atitude, Visão Computacional

Abstract

The employment of embedded cameras in navigation and guidance of Unmanned Aerial Vehicles (UAV) has attracted the focus of many academic researches. In particular, for the multirotor UAV, the camera is widely employed for applications performed at indoor environments, where there are less access to the GNSS signal and higher electromagnetic interference. Nevertheless, in most researches, the images captured by the camera are usually adopted to aid in the linear position/velocity estimation, but not specifically for assisting in the attitude determination process. This dissertation proposes an attitude determination method for multirotor UAVs using pairs of vector measurements taken from one downward facing strapdown camera and angular velocity measurements from gyros. The method consists of three modules. The first detects and identifies landmarks from the captured images. The second module computes the vector measurements related to the direction between the landmarks and the camera. The third module executes the attitude estimation from the vector measurements given by the second module. The employed estimation method consists of a version of the Multiplicative Extended Kalman Filter (MEKF) with sequential update. The proposed method was evaluated via Monte Carlo simulations using Simulink 3D Animation. During the evaluation, the method presented effectiveness and satisfactory results in most of the simulated cases. Finally, future works are suggested for the potential continuation of this research.

Keywords: Aerial Robotics, Kalman Filter, Attitude Determination, Computer Vision

Contents

List of Figures

List of Tables

List of Abbreviations and Acronyms

AD	Attitude Determination
AEKF	Additive Extended Kalman Filter
CA	Center of Area
CCS	Cartesian Coordinate System
CM	Center of Mass
CV	Computer Vision
DoF	Degree of Freedom
EKF	Extended Kalman Filter
FOV	Field Of View
GNSS	Global Navigation Satellite System
SMEKF	Sequential Multiplicative Extended Kalman Filter
KF	Kalman Filter
LS	Least Squares
MEKF	Multiplicative Extended Kalman Filter
MEMS	Microelectromechanical systems
MRP	Modified Rodrigues parameters
MV	Minimum Variance
QUEST	Quaternion Estimator

REQUEST	Recursive QUEST
RGB	Red-Green-Blue color system
SLAM	Simultaneous Localization And Mapping
TRIAD	Tri-Axial Attitude Determination System
UAV	Unmanned Aerial Vehicles
VANT	*Veículo Aéreo Não Tripulado*
VBN	Vision Based Navigation
VTOL	Vertical Take-Off and Landing

List of Symbols

abs[$\bullet$]	Absolute value operator
a2q[$\bullet$]	Conversion operator from Euler Angles 3-1-3 to Quaternion
[$\bullet\times$]	Skew-symmetric matrix
$\check{\bullet}$	Measured value
$\hat{\bullet}$	Estimated value
S_{B}	Body Cartesian coordinate system
S_{G}	Ground Cartesian coordinate system
S_{R}	Reference Cartesian coordinate system
S_{I}	Image Cartesian coordinate system
$\vec{\bullet}$	Geometric vector
i	Landmark index
$\bullet'$	Transposed variable
$\otimes$	Quaternion multiplication operator
$E\,[\bullet]$	Expected value operator
$\mathrm{tr}\,[\bullet]$	Trace operator
$\delta\bullet$	Measurement uncertainty
ϕ	Roll angle
θ	Pitch angle

ψ	Yaw angle
$I_{n\times n}$	$n \times n$ identity matrix
$\mathbf{b}$	Vector measurement related to the body CCS
$\mathbf{r}$	Vector measurement related to the reference CCS
$\mathbf{R}$	Measurement noise covariance matrix
$\mathbf{Q}$	State noise covariance matrix
$\mathbf{D}$	Attitude matrix
$\mathbf{F}$	State model Jacobian
$\mathbf{H}$	Measurement model Jacobian
$\mathbf{a}$	General attitude parameter
$\boldsymbol{\omega}$	Angular velocity
$\mathbf{q}$	Attitude quaternion
$\mathbf{p}$	Modified Rodrigues parameters
$\mathbf{c}$	Landmark color in RGB 0-1 scale
$\mathbf{c}_{\mathrm{d}}$	Detected landmark color in RGB 0-1 scale
$\boldsymbol{\gamma}$	Color comparison index
$\mathbf{p}_{\mathrm{CM}}$	Position of the vehicle CM in S_{G} coordinates
$\mathbf{p}_{\mathrm{LC}}$	Position of the landmark center in S_{G} coordinates
α	Angle between the vector measurement and the camera axis
β	Angle between the image projection of the vector measurement and the X_{I} axis

1 Introduction

The present chapter gives an introduction of the dissertation. Section 1.1 presents the motivation. Section 1.2 presents the bibliographic revision about Attitude Determination (AD) systems and Computer Vision (CV) systems applied in Unmanned Aerial Vehicles (UAV). Section 1.3 explains the scope of this work. Section 1.4 describes the work contribution. Finally, section 1.5 shows the organization this work.

1.1 Motivation

Unmanned Aerial Vehicles are recently common in applications that are risky or expensive for a pilot onboard. Agricultural management (HUANG *et al.*, 2013), topography reconstruction (MANCINI *et al.*, 2013), surveillance and exploration of disaster areas (TAYYAB *et al.*, 2013) and soil erosion monitoring (OLTMANNS *et al.*, 2012), are some examples of the UAV utility. In particular, the multirotor type has shown high versatility for the fore-cited low-altitude applications (KENDOUL; YU; NONAMI, 2010). The hovering and stable low speed flight, vertical take-off and landing (VTOL) and high maneuverability at indoor environments are some of the multirotor UAV characteristics (WANG; YANG, 2012).

Aligned with the recent advances in sensors, actuators, signal processing and control

techniques, the multirotor UAV has shown a growing interest within the academia. The simple mechanics, coupled dynamics and under-actuated characteristics make the control of this device a technological and research challenge (ZHAN; WANG; XI, 2012).

The multirotor UAV needs a feedback controller in order to achieve stability. Typically, the multirotor controller is organized in two loops: the internal loop, concerned with the attitude control, *i.e.* the orientation of the UAV with respect to some reference frame, and the external loop, which is governed by the position controller sending references to the internal one (SANTOS; SAOTOME; CELA, 2013). In order to provide feedback for the attitude controller, an attitude determination system is required. In general, the function of the AD system is to estimate attitude and angular velocity by processing appropriate sensors.

This work is concerned to the multirotor attitude determination based on camera vector measurements. It is motivated by the demand of alternative attitude sensors for urban or indoor applications, where the measurements of magnetometers and Global Navigation Satellite System (GNSS) are unreliable due to electromagnetic interference in the first sensor, or even lack of signal in the later.

The present research was developed in the Aerial Robotics Laboratory (LRA) at the Technological Institute of Aeronautics. The Figure 1.1 shows some of the equipment related to this work.

1.2 State of the Art

This section will present a bibliographic revision about attitude determination methods and the use of computer vision in UAVs.

FIGURE 1.1 – *Laboratório de Robótica Aérea* - LRA.

1.2.1 Attitude Determination in Aerospace Systems

The study of attitude determination systems in the aerospace community has a long history. (WERTZ, 1978) describes the first AD methods, dividing them in two categories: deterministic methods and state estimation methods. Besides this classification, the attitude can be represented by different parameterizations. A survey of attitude representations is seen in (SHUSTER, 1993). Euler angles and quaternions are the preferred ones. Euler angles allows an ease 3D visualization, whereas the quaternions consists of the nonsingular parameterization with the lowest dimensionality.

The main deterministic methods for attitude determination are the QUEST and the TRIAD (SHUSTER; OH, 1981). In these methods, attitude is estimated using only measurements of the present time instant, discarding past measurements. In order to obtain

three-axis attitude, these methods require the observation of at least two vector measurements, *e.g.* gravity and geomagnetic field. If only one vector measurement is obtained, the attitude will be undetermined around its direction.

In principle, state estimation methods can fully determine the attitude from only one vector measurement. However this vector has to change sufficiently fast. This is justified by the use of past and present measurements together with prior attitude information. These methods are divided into two groups depending on their underlying optimal criteria: Least Squares (LS) and Minimum Variance (MV). Examples of quaternion estimation using the LS approach can be seen in (BAR-ITZHACK, 1996) and (CHOUKROUN; BAR-ITZHACK; OSHMAN, 2004). The Additive Extended Kalman Filter (AEKF) (BAR-ITZHACK; OSHMAN, 1985) and the Multiplicative Extended Kalman Filter (MEKF) (LEFFERTS; MARKLEY; SHUSTER, 1982) are examples of MV methods using quaternion, while the reference (FARRELL, 1970) presents a MV method for estimation of Euler angles.

The low-cost microelectromechanical systems (MEMS) are adopted in most multirotor UAVs. However their measurements are quite noisy and require auxiliary sensors for bounding its crescent errors. Moreover, the MEMS accelerometer senses the vibration and lateral acceleration of the UAV, which impedes the gravity vector to be precisely measured. The reference (GEBRE-EGZIABHER; ELKAIM, 2008) uses magnetometers, accelerometers and GPS for attitude estimation. Its estimator uses GPS calculated acceleration for correcting the gravity estimate from the accelerometers. In attempt to mitigate the problem of noisy accelerometer measurements, (KIM; KIM; LYOU, 2012) proposes a second order infinite impulse response (IIR) notch filter for rejecting the effects of vibration on the accelerometer measurements. Kalman filter approaches for multirotor attitude estimation can be found in (WANG; YANG, 2012) and (HOFFMANN; GODDEMEIER; BERTRAM, 2010).

Although it is known that multirotors for professional applications uses Kalman filter for attitude estimation, there are few references about this subject.

1.2.2 Navigation and Attitude Determination Using Computer Vision

Computer Vision systems can be used either as a secondary sensor, complementing Inertial Navigation System (INS), or as the main sensor, in Vision Based Navigation (VBN). The first option is adopted for bounding the crescent INS error (CHEVIRON *et al.*, 2007),(ERGINER; ALTUG, 2007), (CARRILLO *et al.*, 2012). For the VBN, the main interest is to develop a navigation system based on visual references (TOURNIER *et al.*, 2006), (BLOSCH *et al.*, 2010).

(CHEVIRON *et al.*, 2007) proposed a filtering algorithm that fuses inertial data from accelerometers and gyrometers with a camera in order to obtain the pose and speed of a helicopter UAV. In their experiment, the camera is strapdown and faces one target with known position in the floor. The measured images contain the position and orientation of the camera with respect to a reference frame fixed on the ground. Two estimators are presented; the first one estimates both angular position and angular velocity bias, while the second estimates the linear position and speed. Using the same idea, (ERGINER; ALTUG, 2007) utilized the landing pad as target. Their algorithm extracted the relative position of the edges of the landing pad with respect to the quadrotor UAV in order to feed a proportional-derivative (PD) controller. (CARRILLO *et al.*, 2012) proposed a forward stereoscopic vision system to aid the INS. In their work, both angular and linear speeds were computed using the stereo visual odometry. This method consists in the calculus

of the disparity between the right and left images, allowing the computation of the scene depth frame by frame. Vision data are fused with the INS data by means of a Kalman filter.

A VBN approach is found in (TOURNIER *et al.*, 2006). It uses Moiré patterns inside the camera‘s target in order to increase the accuracy of the position estimator. The Moiré patterns move in the same direction of the camera, however in a greater scale. This displacement is sensed by the camera, resulting in a better identification and resolution of the UAV position. A Simultaneous Localization And Mapping (SLAM) application is presented in (BLOSCH *et al.*, 2010). It uses the algorithm presented by (KLEIN; MURRAY, 2007), which separates the SLAM task in two operations: tracking and mapping. The division allows the UAV pose to be computed independently in the first operation, followed by the point map creation in the second.

In the CV literature, few works are concerned to attitude determination. The reference (SHABAYEK *et al.*, 2012) lists methods based on horizon detection, vanishing points, optical flow and stereo vision. For indoor and urban applications, we can highlight (TARHAN; ALTUG, 2011). It adopts a catadioptric optical system for attitude estimation. This system is composed by curved mirrors and lenses disposed in order to visualize a hemispherical image. The main idea is to obtain the rotation matrix that relates two consecutive vanishing directions, which is the homography matrix, for extracting the attitude angles. In this work, an EKF is used to estimate the position and velocity of the UAV.

1.3 Scope

The present work is aimed at proposing a multirotor attitude determination method on the base of the experienced literature on satellite attitude determination from vector measurements. The vector measurements commonly used in attitude determination of satellites are taken from solar sensors (Sun direction), magnetometers (local geomagnetic field vector), horizon sensors (direction of nadir) and star sensors (direction of stars). Differently, our strategy is to take vector measurements from one strapdown camera visualizing landmarks on the ground. This strategy allows the computation of non-colinear vectors, which will be used together with angular velocity measurements in an EKF-like filter for attitude determination.

1.4 Contribution of the Dissertation

The contributions of this work are:

- *An attitude determination method using vector measurements taken from one downward strapdown camera.* This method consists of three parts: The first part detects and identifies the landmarks, the second part provides the unit vectors pointing from the vehicle to identified landmarks, the last part estimates the attitude from the identified unit vectors.

- *A sequential version of the Multiplicative Extended Kalman Filter (MEKF).* The number of iterations of the filter algorithm is adjusted according to the quantity of identified vector measurements. As benefit, the sequential MEKF automatically adapts from one to nine vector measurements in our case and, moreover, has lower

dimension matrices for estimating the attitude.

- *Evaluation of the proposed method using simulation.* In order to give visualization to the simulation, this work resorted to Simulink 3D Animation. The idealized environment is a quadrotor model hovering over nine landmarks. In this simulation, the vehicle has only angular movements as we are only concerned with the attitude estimation.

1.5 Text Organization

The remaining text of this dissertation is organized in the following manner:

- **Chapter 2**. Defines the attitude determination problem from pairs of vector measurements taken from one downward facing strapdown camera;
- **Chapter 3**. Describes the problem solution by a block diagram. It presents the formulation for detection and identification of landmarks, the construction of unit vector measurements and the sequential version of multiplicative Kalman filter;
- **Chapter 4**. Presents the simulation environment and the evaluation of the method via Monte Carlo simulation;
- **Chapter 5**. Concludes the work and suggests future research and applications.

2 Problem Statement

In the following, Section 2.1 defines a problem of attitude determination for multirotor vehicle using pairs of vector measurements taken from a downward strapdown camera. Section 2.2 shows some comments regarding the defined problem.

2.1 Attitude Determination Problem

Consider the multirotor helicopter and three Cartesian Coordinate Systems (CCS) illustrated in Fig. 2.1. The body CCS $S_{\mathrm{B}} = \{X_{\mathrm{B}},Y_{\mathrm{B}},Z_{\mathrm{B}}\}$ is attached to the vehicle at its Center of Mass (CM). The ground CCS $S_{\mathrm{G}} = \{X_{\mathrm{G}},Y_{\mathrm{G}},Z_{\mathrm{G}}\}$ is fixed on the ground at point O. The reference CCS $S_{\mathrm{R}} = \{X_{\mathrm{R}},Y_{\mathrm{R}},Z_{\mathrm{R}}\}$ is parallel to S_{G} but is centered at CM.

Assume that the camera is positioned at the CM and the triad of rate-gyros is aligned with S_{B}. Define the set of landmark indexes to be $\mathcal{I} \triangleq \{1,2,...,l\}$. Denote the center of the i-th landmark by $M^{(i)}$. Define $\vec{\mathbf{s}}^{(i)}$ to be the unit geometric vector pointing from CM to $M^{(i)}$. Denote the representations of $\vec{\mathbf{s}}^{(i)}$ in S_{B} and S_{R} by $\mathbf{b}^{(i)} \in \mathbb{R}^3$ and $\mathbf{r}^{(i)} \in \mathbb{R}^3$, respectively. The representations $\mathbf{b}^{(i)}$ and $\mathbf{r}^{(i)}$ are interrelated by $\mathbf{b}^{(i)} = \mathbf{D}\mathbf{r}^{(i)}$, where $\mathbf{D} \in SO(3)$ is the attitude matrix of S_{B} with respect to S_{R}. In order to measure at least one pair $(\mathbf{b}^{(i)},\mathbf{r}^{(i)})$, one assumes that both CM and landmarks have known positions with

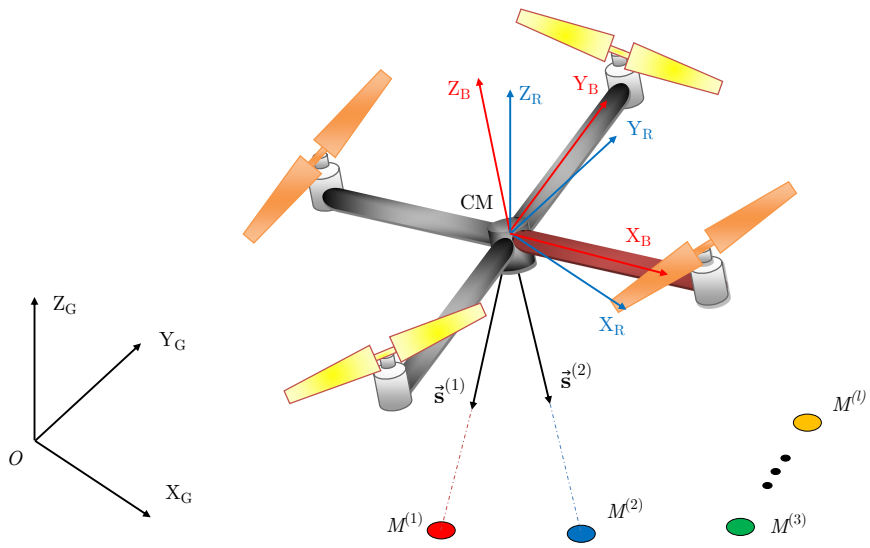

FIGURE 2.1 – The Cartesian coordinate systems and the flight environment.

respect to S_{G}. This yields the following sequence of noncollinear vector measurements:

$$\mathcal{V}_k \triangleq \left\{ \left(\check{\mathbf{b}}_k^{(i_1)}, \check{\mathbf{r}}_k^{(i_1)} \right), \left(\check{\mathbf{b}}_k^{(i_2)}, \check{\mathbf{r}}_k^{(i_2)} \right), \ldots, \left(\check{\mathbf{b}}_k^{(i_m)}, \check{\mathbf{r}}_k^{(i_m)} \right) \right\}, \tag{2.1}$$

for $\{i_1, i_2, \ldots, i_m\} \subset \mathcal{I}, i_1 \neq i_2 \neq \ldots \neq i_m$, where $\check{\mathbf{b}}_k^{(i)}$ and $\check{\mathbf{r}}_k^{(i)}$ are respective samples of $\mathbf{b}^{(i)}$ and $\mathbf{r}^{(i)}$ at the discrete time instant k and $m \in \mathcal{I}$, is the number of measured vectors. Note that m is the number of landmarks detected by the camera at each instant k.

Therefore, from the vector measurements $\mathcal{V}_k$, one could propose the following measurement model:

$$\check{\mathbf{b}}_k^{(i)} = \mathbf{D}(\mathbf{d}_k)\mathbf{r}_k^{(i)} + \delta\mathbf{b}_k^{(i)}, \tag{2.2}$$

$$\check{\mathbf{r}}_k^{(i)} = \mathbf{r}_k^{(i)} + \delta\mathbf{r}_k^{(i)}, \tag{2.3}$$

for $i = i_1, i_2, \ldots, i_m$, where $\{\delta\mathbf{b}_k^{(i)}\}$ and $\{\delta\mathbf{r}_k^{(i)}\}$ are zero-mean Gaussian white sequences

with covariances $\mathbf{R}_{b,k}^{(i)}$ and $\mathbf{R}_{r,k}^{(i)}$, respectively, and $\mathbf{d}_k \in \mathbb{R}^n$ is a discrete-time attitude representation vector which parameterizes the attitude matrix $\mathbf{D}(\mathbf{d}_k)$.

The attitude kinematics is modeled by the following differential equation (WERTZ, 1978):

$$\dot{\mathbf{d}}(t) = \mathbf{f}(\mathbf{d}(t),\boldsymbol{\omega}(t)), \tag{2.4}$$

where $\mathbf{d}(t)$ is a continuous-time version of $\mathbf{d}_k$, $\boldsymbol{\omega}(t) \in \mathbb{R}^3$ is the true angular velocity of S_{B} with respect to S_{R}, represented in S_{B}.

Let the measurement taken from the rate-gyros at the discrete-time instant k be described by the following stochastic model:

$$\check{\boldsymbol{\omega}}_k = \boldsymbol{\omega}_k + \delta\boldsymbol{\omega}_k, \tag{2.5}$$

where $\boldsymbol{\omega}_k \in \mathbb{R}^3$ is a sample of $\boldsymbol{\omega}(t)$ at the discrete-time instant k, $\delta\boldsymbol{\omega}_k \in \mathbb{R}^3$ is the rate-gyro measurement noise, which is assumed to be a zero-mean Gaussian white sequence $\{\delta\boldsymbol{\omega}_k\}$ with covariance $\mathbf{Q}$.

The main problem of the present work is to recursively compute an approximation $\hat{\mathbf{d}}_{k|k}$ of the minimum-variance (MV) estimate of $\mathbf{d}_k$ using the dynamic equation (2.4), the measurement equations (2.2)-(2.3) as well as the measurements $\check{\boldsymbol{\omega}}_{1:k}$, and $\mathcal{V}_{1:k}$.

2.2 Comments

The present section has defined the attitude determination problem as a minimum variance estimation problem with arbitrary attitude parameter. The peculiar characteristic of the present problem is the use of one camera for acquiring information in order to

define unitary vector measurements. It has to be clear that the index m represents the quantity of computed vector measurements for one specific image frame. Therefore, the corresponding m landmarks had to be available in the camera FOV in order to allow the image processing and further measurement computation. The next chapter will present a solution for the aforementioned problem substituting the arbitrary attitude parameter by modified Rodrigues parameters.

3 Problem Solution

The current section presents a solution for the Attitude Determination problem defined in Section 2.1. In the following, Section 3.1 presents the organization of the method. Section 3.2 presents the landmark detection and identification algorithm. Section 3.3 describes the construction of vector measurement pairs. Section 3.4 proposes a sequential version of the Multiplicative Extended Kalman Filter for attitude estimation. Finally, Section 3.5 presents some comments regarding the proposed solution.

3.1 The Attitude Determination Method

The attitude determination method presented in this work is organized in three modules. Each module is, respectively, represented by one block in the diagram of Figure 3.1. Block 1 computes the landmark position in the image CCS S_{I}[1] given the captured images and the landmark colors. Block 2 constructs the vector measurement pairs given the multirotor position in S_{G} and the landmark positions in S_{I}. Block 3 estimates the multirotor attitude given the vector measurements together with the vehicle‘s angular velocity measurements.

The block diagram of Figure 3.1 is general in the sense that each block can be im-

[1] S_{I} will be defined in Section 3.2.

plemented by alternative algorithms. For block 1, edge detection algorithms such as Kayyali, Canny and Sobel, are examples that could be implemented for landmark detection and identification. For block 2 it is possible to equate different mathematical models for computing unit vector measurements. For block 3, it is possible to implement the AD methods from references (SHUSTER; OH, 1981), (BAR-ITZHACK; OSHMAN, 1985), (BAR-ITZHACK, 1996) and (IDAN, 1996), just to cite some examples.

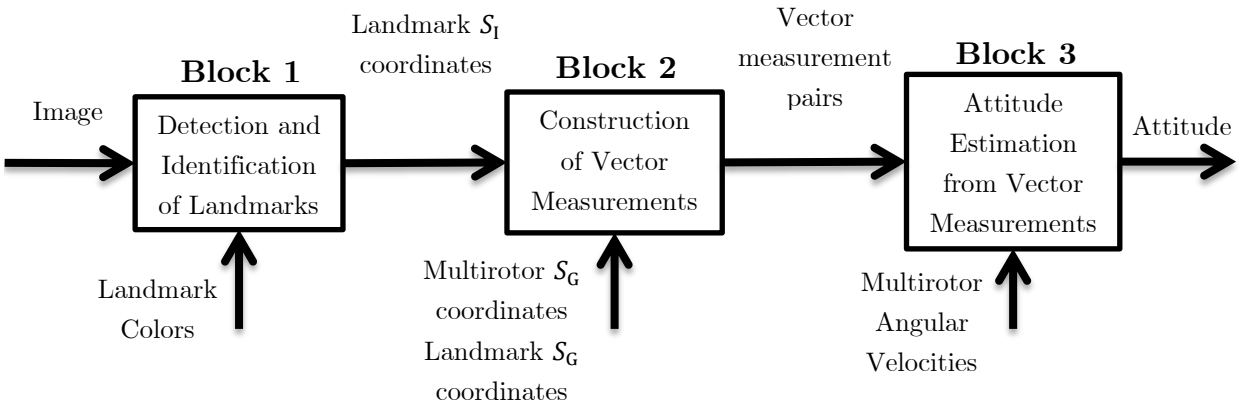

FIGURE 3.1 – Block diagram of the overall attitude determination method.

The following three sections will detail our choice for each block of the overall system illustrated in Figure 3.1.

3.2 Block 1: Detection and Identification of Landmarks

This block detects and identifies the landmarks placed inside the camera FOV classifying the color of each landmark. A comparison between the stored landmark color and each pixel of the captured image recognize the landmark in the image.

Let $\mathbf{c}^{(i)}$ define the color of the i-th landmark in RGB 24 bits placed in the unitary scale, as follows:

$$\mathbf{c}^{(i)} = \frac{\begin{bmatrix} R & G & B \end{bmatrix}'}{256}, \tag{3.1}$$

where R, G and B are the colors components red, green and blue, respectively. The 24 bits color range allows 256 intensity levels for each color component. In order to place the color components in a unitary scale, it is necessary to divide each color component by 256, which justifies the denominator of equation (3.1). The result of equation (3.1) is stored in the algorithm of the block 1. Let $\mathbf{c}_d(x,y)$ define the color in the unitary scale of a detected pixel in the image matrix, where x and y are the pixel coordinates in the image CCS $S_{\mathrm{I}} = \{X_{\mathrm{I}},Y_{\mathrm{I}}\}$ as shown in Figure 3.2. $\mathbf{c}_d(x,y)$ is computed in the same manner of equation (3.1). Assuming no repeated color between each landmark and, moreover, the floor has a different color from all landmarks, the landmark recognition is given by the following comparison:

$$\boldsymbol{\gamma}_{\mathbf{c}}^{(i)} = \mathrm{abs}\left[\mathbf{c}^{(\mathrm{i})} - \mathbf{c}_{\mathrm{d}}(\mathrm{x,y})\right], \tag{3.2}$$

where abs is the absolute value operator. In order to execute a exhaustive comparison, for each pixel (x,y), the index (i) assumes a new value until all landmark colors are compared to the current $\mathbf{c}_d(x,y)$. Furthermore, the coordinates (x,y) of the pixel assumes a new value until all image had been compared.

Assume the pixel coordinates (x,y) to advance in ascending order in y and then in x, necessarily in this order. One can state that the (x,y) coordinates of the first detected pixel are in the opposite corner of the last detected pixel, as show in Figure 3.2.

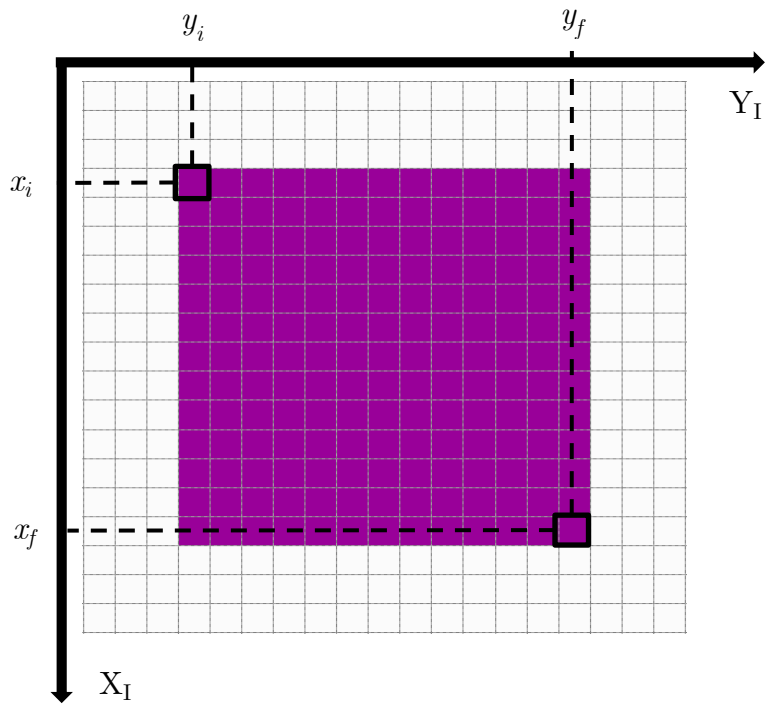

FIGURE 3.2 – The position of the first and last pixels detected in a square landmark.

Assume all landmarks to be squares as shown in Figure 3.2. The approximated coordinate of the center of the landmark is given by:

$$\mathbf{v}_{\mathrm{I}} = \begin{bmatrix} \dfrac{x_f + x_i}{2} \\ \dfrac{y_f + y_i}{2} \end{bmatrix}, \tag{3.3}$$

where sub-indexes i and f respectively denotes the initial and the final coordinates in pixels of the detected landmark in the S_{I} system.

The illumination of the scene may interfere in the result of the comparison index $\boldsymbol{\gamma}_{\mathbf{c}}^{(i)}$. Even though the vector $\mathbf{c}_d(x,y)$ corresponds to a landmark, the color intensity can differ from the correspondent stored landmark color. Define $\boldsymbol{\tau} \in \mathbb{R}^3$ as a parameter related to the scene illumination. The value of $\boldsymbol{\tau}$ is manually tuned in order to allow the landmark recognition for $\boldsymbol{\gamma}_{\mathbf{c}}^{(i)} \leqslant \boldsymbol{\tau}$.

3.3 Block 2: Construction of Vector Measurements

The present section demonstrates one possible manner to compute a pair of unit vectors **(b, r)** pointing from the CM of the vehicle to the center of the landmark using images taken from the embedded camera. The Figure 3.3 shows the necessary projections for obtaining the desired vector measurement using the downward facing camera and one landmark inside its FOV.

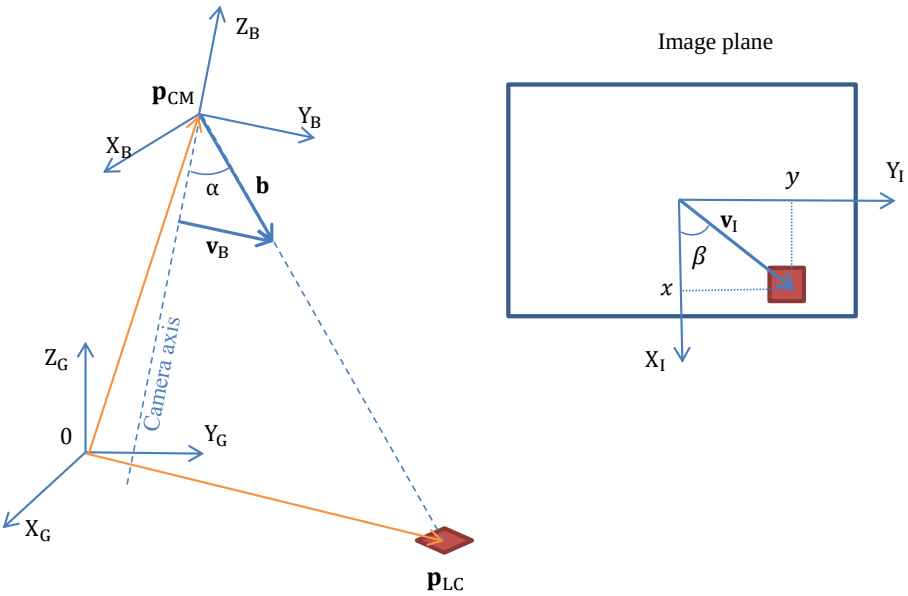

FIGURE 3.3 – Vector measurements representation.

Let $\mathbf{p}_{\mathrm{LC}}$ and $\mathbf{p}_{\mathrm{CM}}$ denote the S_{G} representation of the landmark‘s center and the vehicle‘s center of mass, respectively. The vector $\mathbf{r}$ can be easily obtained by:

$$\mathbf{r} = \frac{\mathbf{p}_{\mathrm{LC}} - \mathbf{p}_{\mathrm{CM}}}{\|\mathbf{p}_{\mathrm{LC}} - \mathbf{p}_{\mathrm{CM}}\|}. \tag{3.4}$$

In order to obtain the vector $\mathbf{b}$, the first step is to calculate the vector $\mathbf{v}_{\mathrm{I}}$, which is

the landmark position along the image plane X_{I}-Y_{I}. It is important to mention that $||\mathbf{v}_{\mathrm{I}}||$ is an exclusive function of the α angle. Note that, if the landmark moves along the line $\overline{p_{\mathrm{LC}}p_{\mathrm{CM}}}$, $||\mathbf{v}_{\mathrm{I}}||$ remains the same. As shown in Figure 3.3, it is possible to obtain the direction of $\mathbf{v}_{\mathrm{I}}$ from the image using

$$\cos(\beta) = \frac{x}{||\mathbf{v}_{\mathrm{I}}||}, \tag{3.5}$$

$$\sin(\beta) = \frac{y}{||\mathbf{v}_{\mathrm{I}}||}, \tag{3.6}$$

where x and y are the coordinates of the landmark center in pixels. Considering the axes X_{I} and Y_{I} parallel to X_{B} and Y_{B}, respectively, and denoting $\mathbf{v}_{\mathrm{B}}$ as the projection of $\mathbf{b}$ in the X_{B}-Y_{B} plane, one can ensure that

$$||\mathbf{v}_{\mathrm{B}}|| = j||\mathbf{v}_{\mathrm{I}}||, \tag{3.7}$$

where j is the conversion parameter from pixels to meters. Note that j depends on the camera focus, which is calibrated according to the vehicle height. Using trigonometry, it is possible to find α by

$$\alpha = \mathrm{asin}(||\mathbf{v}_{\mathrm{B}}||). \tag{3.8}$$

Reminding that $\mathbf{b}$ is unitary, it can be finally obtained by:

$$\mathbf{b} = \begin{bmatrix} \sin(\alpha)\cos(\beta) & \sin(\alpha)\sin(\beta) & \cos(\alpha) \end{bmatrix}'. \tag{3.9}$$

3.4 Block 3: Attitude Estimation from Vector Measurements

The Multiplicative Extended Kalman Filter was firstly proposed by (LEFFERTS; MARKLEY; SHUSTER, 1982). The MEKF represents the global attitude in quaternions while estimates the attitude error using a three-dimensional attitude parameterization (MARKLEY, 2003). The main characteristic of the MEKF is to maintain the unit norm of the attitude quaternion during the update of the filter. The algorithm proposed in the following is based on the MEKF and, as contribution, sequentially processes the vector measurements in the update step of the filter. Due to the sequential iterations during the update step, the proposed method is named Sequential Multiplicative Extended Kalman Filter (SMEKF).

As well as the MEKF proposed by the reference (MARKLEY; CRASSIDIS, 1996), this work represents the true attitude quaternion by

$$\mathbf{q}(t) = \delta\mathbf{q}(\mathbf{p}(t)) \otimes \hat{\mathbf{q}}(t), \tag{3.10}$$

where $\hat{\mathbf{q}}(t)$ is a reference quaternion, $\delta\mathbf{q}(\mathbf{p}(t))$ is the multiplicative error quaternion parameterized by modified Rodrigues parameters (MRP) $\mathbf{p}(t)$, and $\otimes$ denotes the quaternion product (SHUSTER, 1993). The reference quaternion $\hat{\mathbf{q}}(t)$ is considered the best estimate of the true quaternion $\mathbf{q}(t)$ between the interval $[t_k,t_{k+1})$. Thus, the MRP assumes

$$\mathbf{p}(t) = 0 \;\; \forall \;\; t \in [t_k,t_{k+1}), \tag{3.11}$$

which eliminates the redundancy of using two paramerizations.

Let the state model defined by equation (2.4) be redefined in MRP as follows:

$$\dot{\mathbf{p}}(t) = \mathbf{G}(\mathbf{p}(t))\breve{\boldsymbol{\omega}}(t) + \mathbf{G}(\mathbf{p}(t))\delta\boldsymbol{\omega}(t), \tag{3.12}$$

where $\mathbf{p}(t) \triangleq \begin{bmatrix} p_{1,t} & p_{2,t} & p_{3,t} \end{bmatrix}'$ is the MRP vector, $\breve{\boldsymbol{\omega}}(t) \in \mathbb{R}^3$ is the measured angular velocity, $\delta\boldsymbol{\omega}(t) \in \mathbb{R}^3$ is the rate-gyro measurement noise, which is assumed to be a zero-mean Gaussian white sequence $\{\delta\boldsymbol{\omega}(t)\}$ with covariance $\mathbf{Q}$, and $\mathbf{G}(\mathbf{p}(t))$ is defined by (SCHAUB,) in the following form:

$$\mathbf{G}(\mathbf{p}(t)) = \frac{1}{4}\left\{(1 - ||\mathbf{p}(t)||^2)\mathbf{I}_3 + 2[\mathbf{p}(t)\times] + 2\mathbf{p}(t)\mathbf{p}(t)'\right\}. \tag{3.13}$$

Assuming $\{\mathbf{p}(t)\}$ and $\{\delta\boldsymbol{\omega}(t)\}$ to be statistically independents, the mean $E\left[\mathbf{G}(\mathbf{p}(t))\delta\boldsymbol{\omega}(t)\right]$ is null. The covariance $E\left[(\mathbf{G}(\mathbf{p}(t+\tau))\delta\boldsymbol{\omega}(t+\tau))(\mathbf{G}(\mathbf{p}(t))\delta\boldsymbol{\omega}(t))'\right] = \mathbf{Q}^{\mathbf{p}}(t)\delta(\tau)$ has unknown value related to the true state. In order to implement the filter, the covariance of the state noise is approximated by:

$$\mathbf{Q}^{\mathbf{p}}(t) = \boldsymbol{\Gamma}(t)\mathbf{Q}\boldsymbol{\Gamma}(t)', \tag{3.14}$$

where $\boldsymbol{\Gamma}(t) = \mathbf{G}(\hat{\mathbf{p}}(t))$, $\forall t \in [t_k, t_{k+1})$.

In order to execute the state propagation, the nonlinear function given by equation (3.12) is expanded in Taylor series around the latest estimate $\hat{\mathbf{p}}(t)$. For the present work, it is adopted the first order EKF, which neglects higher order terms (HOT) after the expansion. Applying the first order Taylor series expansion in the first term of equation

(3.12), results:

$$f\left(\mathbf{p}(t),\check{\boldsymbol{\omega}}(t)\right) = f\left(\hat{\mathbf{p}}(t),\check{\boldsymbol{\omega}}(t)\right) + \left.\frac{\partial f\left(\mathbf{p}(t),\check{\boldsymbol{\omega}}(t)\right)}{\partial \mathbf{p}}\right|_{\mathbf{p}=\hat{\mathbf{p}}(t)} \left(\mathbf{p}(t) - \hat{\mathbf{p}}(t)\right) + \mathrm{HOT}, \tag{3.15}$$

where

$$f\left(\mathbf{p}(t),\check{\boldsymbol{\omega}}(t)\right) = \mathbf{G}(\mathbf{p}(t))\check{\boldsymbol{\omega}}(t) \tag{3.16}$$

From equation (3.15), the following Jacobian is defined:

$$\mathbf{F}(\hat{\mathbf{p}}(t),\check{\boldsymbol{\omega}}(t)) \triangleq \left.\frac{\partial \mathbf{G}(\mathbf{p}(t))\check{\boldsymbol{\omega}}(t)}{\partial \mathbf{p}}\right|_{\mathbf{p}=\hat{\mathbf{p}}(t)}. \tag{3.17}$$

The partial derivatives of equation (3.17) results in the following:

$$\left.\frac{\partial \mathbf{G}(\mathbf{p}(t))\check{\boldsymbol{\omega}}(t)}{\partial \mathbf{p}}\right|_{\mathbf{p}=\hat{\mathbf{p}}(t)} = \frac{1}{2}\left\{\hat{\mathbf{p}}(t)\check{\boldsymbol{\omega}}(t)' - \check{\boldsymbol{\omega}}(t)\hat{\mathbf{p}}(t)' - [\check{\boldsymbol{\omega}}\times] + \left(\check{\boldsymbol{\omega}}(t)'\hat{\mathbf{p}}(t)\right)\mathbf{I}_3\right\}. \tag{3.18}$$

The equation (3.18) can be simplified using the assumption given by equation (3.11), which yields into:

$$\mathbf{F}(\hat{\mathbf{p}}(t),\check{\boldsymbol{\omega}}(t)) = \frac{1}{2}(-[\check{\boldsymbol{\omega}}\times]). \tag{3.19}$$

Let the discrete-time measurement model be defined by

$$\check{\mathbf{b}}_k^{(i)} = \mathbf{D}(\mathbf{q}_k)\mathbf{r}_k^{(i)} + \delta\mathbf{b}_k^{(i)}, \tag{3.20}$$

where $\mathbf{r}_k^{(i)}$ is the discrete time vector measurement in S_{R}, $\{\delta\mathbf{b}_k^{(i)}\}$ is a zero-mean Gaussian white sequence with covariance $\mathbf{R}_{b,k}^{(i)}$ and $\mathbf{D}(\mathbf{q}_k)$ is true attitude matrix in quaternions, given by (SHUSTER, 1993):

$$\mathbf{D}(\mathbf{q}_k) = (q_{1,k}^2 - |\mathbf{e}_k|^2)\mathbf{I}_3 + 2\mathbf{e}_k\mathbf{e}_k' - 2q_{1,k}[\mathbf{e}_k\times], \tag{3.21}$$

where $q_{1,k}$ and $\mathbf{e}_k$ are the scalar and vector part of the quaternion, respectively.

It is necessary manipulate the terms of equation (3.20) in order to represent the attitude error in MRP. The equation (3.10) leads to equation (3.21) to the following property:

$$\mathbf{D}(\mathbf{q}_k) = \mathbf{D}(\delta\mathbf{q}_k)\mathbf{D}(\hat{\mathbf{q}}_k), \tag{3.22}$$

where $\mathbf{D}(\delta\mathbf{q}_k)$ is the attitude error matrix and $\mathbf{D}(\hat{\mathbf{q}}_k)$ is the estimated global attitude matrix. Since the attitude error $\delta\mathbf{q}_k$ is actually parameterized by $\hat{\mathbf{p}}_k$, the following equivalence is true:

$$\mathbf{D}(\delta\mathbf{q}_k) = \mathbf{D}(\hat{\mathbf{p}}_k), \tag{3.23}$$

where

$$\mathbf{D}(\hat{\mathbf{p}}_k) = \mathbf{I}_3 + \frac{8[\hat{\mathbf{p}}_k\times]^2 - 4(1 - \|\hat{\mathbf{p}}_k\|^2)[\hat{\mathbf{p}}_k\times]}{(1 + \|\hat{\mathbf{p}}_k\|^2)^2} \tag{3.24}$$

is the attitude matrix in MRP.

Substituting equation (3.23) into (3.20), results:

$$\check{\mathbf{b}}_k^{(i)} = \mathbf{D}(\hat{\mathbf{p}}_k)\mathbf{D}(\hat{\mathbf{q}}_k)\mathbf{r}_k^{(i)} + \delta\mathbf{b}_k^{(i)}, \tag{3.25}$$

where $\mathbf{D}(\hat{\mathbf{q}}_k)\mathbf{r}_k^{(i)} \triangleq \overline{\mathbf{b}}_k^{(i)}$. Similarly to the state propagation, it is necessary to expand the first term of equation (3.25) in first order Taylor series, as follows:

$$h\left(\mathbf{p}_k, \overline{\mathbf{b}}_k^{(i)}\right) = h\left(\hat{\mathbf{p}}_k, \overline{\mathbf{b}}_k^{(i)}\right) + \left.\frac{\partial h\left(\mathbf{p}_k, \overline{\mathbf{b}}_k^{(i)}\right)}{\partial \mathbf{p}}\right|_{\mathbf{p}=\hat{\mathbf{p}}_{k+1|k}} (\mathbf{p}_k - \hat{\mathbf{p}}_k), \tag{3.26}$$

where

$$h\left(\mathbf{p}_k, \overline{\mathbf{b}}_k^{(i)}\right) = \mathbf{D}(\mathbf{p}_k)\overline{\mathbf{b}}_k^{(i)}. \tag{3.27}$$

From equation (3.26), it is possible to define the following Jacobian matrix:

$$\mathbf{H}_{\mathbf{p},k+1}^{(i)} \triangleq \left.\frac{\partial \mathbf{D}(\mathbf{p}_k)\overline{\mathbf{b}}_k^{(i)}}{\partial \mathbf{p}}\right|_{\mathbf{p}=\hat{\mathbf{p}}_{k+1|k}}, \tag{3.28}$$

where equation (3.24) is used for the derivatives and results in the following:

$$\mathbf{H}_{\mathbf{p},k+1}^{(i)} = \frac{4}{(1+\hat{\mathbf{p}}'\hat{\mathbf{p}})^2}\left[\overline{\mathbf{b}}_k^{(i)}\times\right]\left\{(1+\hat{\mathbf{p}}'\hat{\mathbf{p}})I_{3\times3} - 2[\hat{\mathbf{p}}\times] + 2\hat{\mathbf{p}}\hat{\mathbf{p}}'\right\}, \tag{3.29}$$

for $\hat{\mathbf{p}} = \hat{\mathbf{p}}_{k+1|k}$. It is possible to simplify equation (3.29) using equation (3.11), which yields into:

$$\mathbf{H}_{\mathbf{p},k+1}^{(i)} = 4\left[\overline{\mathbf{b}}_k^{(i)}\times\right]. \tag{3.30}$$

Since the global attitude is represented in quaternions, the SMEKF uses the quaternion kinematic equation in the interval $[t_k,t_{k+1})$ for propagating the attitude, as follows:

$$\hat{\mathbf{q}}_{k+1|k} = \mathrm{e}^{\check{\mathbf{\Omega}}_k \mathrm{T_s}} \hat{\mathbf{q}}_{k|k}, \tag{3.31}$$

where T_s is the sampling time and

$$\check{\mathbf{\Omega}}_k = \frac{1}{2} \begin{bmatrix} 0 & -\check{\boldsymbol{\omega}}'_k \\ \check{\boldsymbol{\omega}}_k & -[\check{\boldsymbol{\omega}}_k \times] \end{bmatrix}. \tag{3.32}$$

Given the estimated attitude error in MRP, it is necessary to apply the conversion to attitude quaternion, as follows

$$\delta\mathbf{q}(\mathbf{p}_{k+1|k+1}) = \begin{bmatrix} \dfrac{1 - ||\mathbf{p}_{k+1|k+1}||^2}{1 + ||\mathbf{p}_{k+1|k+1}||^2} \\ \dfrac{2p_{1,k+1|k+1}}{1 + ||\mathbf{p}_{k+1|k+1}||^2} \\ \dfrac{2p_{2,k+1|k+1}}{1 + ||\mathbf{p}_{k+1|k+1}||^2} \\ \dfrac{2p_{3,k+1|k+1}}{1 + ||\mathbf{p}_{k+1|k+1}||^2} \end{bmatrix}. \tag{3.33}$$

The update of the global attitude is executed using a discrete-time version of equation (3.10), as shown in the following:

$$\delta\mathbf{q}(\mathbf{p}_{k+1|k+1}) \otimes \hat{\mathbf{q}}_{k+1|k} = \begin{bmatrix} \delta q_1 \hat{q}_1 - \delta\mathbf{e} \bullet \hat{\mathbf{e}} \\ \hat{q}_1 \delta\mathbf{e} + \delta q_1 \hat{\mathbf{e}} - \delta\mathbf{e} \times \hat{\mathbf{e}} \end{bmatrix}, \tag{3.34}$$

where δq_1 and $\delta\mathbf{e}$ represent the scalar part and the vector part of $\delta\mathbf{q}(\mathbf{p}_{k+1|k+1})$, while $\hat{q}_1$ and $\hat{\mathbf{e}}$ represent the scalar part and the vector part of $\hat{\mathbf{q}}_{k+1|k}$, respectively.

The main characteristic of SMEKF is to sequentially compute the measurement prediction and update steps for each vector measurement. Differently, the original MEKF processes all vector measurements at the same loop for updating the estimation. Given the k instant vector measurements, the attitude error $\hat{\mathbf{p}}_{k+1|k+1}$ is gradually updated before the attitude reset in equation (3.10). Equation (3.35) presents the sequential estimation update of SMEKF.

$$\hat{\mathbf{p}}^{(i)}_{k+1|k+1} = \hat{\mathbf{p}}^{(i-1)}_{k+1|k} + \mathbf{K}_{k+1}\left(\mathbf{b}^{(i)}_{k+1} - \overline{\mathbf{b}}^{(i)}_{k+1|k}\right), \tag{3.35}$$

where $\hat{\mathbf{p}}^{(i-1)}_{k+1|k+1}$ defines the error in MRP given the $(i-1)$ vector measurement. Note that the SMEKF also needs at least two vector measurements in order not to diverge the attitude estimation.

The sequential characteristic of the SMEKF allows the filter to use equation (3.20) one time for each measurement, fixing the dimension of equation (3.28) in 3×3. The measurement noise covariance $\mathbf{R}_{k+1}$ also has fixed dimension in 3×3. Diferently, the MEKF adds 3 rows in equation (3.28) and 3×3 covariances in $\mathbf{R}_{k+1}$ for each vector measurement.

Organizing the equations developed until this point of the text, it is possible to define the SMEKF. In the same manner of the Multiplicative Extended Kalman Filter, the state and measurement equations are given by (3.12) and (3.20), respectively. Table 3.1 summarizes the algorithm of the SMEKF.

TABLE 3.1 – SMEKF algorithm.

Initial conditions	$\hat{\mathbf{q}}_{0\|0} = \hat{\mathbf{q}}_0$ $\mathbf{P}^{\mathbf{p}}_{0\|0} = \mathbf{P}^{\mathbf{p}}_0$ $\hat{\mathbf{p}}^{(0)}_{0\|0} = 0$
State propagation	$\hat{\mathbf{p}}(t) = 0, t \in [t_k, t_{k+1})$ $\dot{\mathbf{P}}^{\mathbf{p}}(t) = \mathbf{F}(\hat{\mathbf{p}}(t), \breve{\boldsymbol{\omega}}(t))\mathbf{P}^{\mathbf{p}}(t) + \mathbf{P}^{\mathbf{p}}(t)\mathbf{F}(\hat{\mathbf{p}}(t), \breve{\boldsymbol{\omega}}(t))' + \mathbf{Q}^{\mathbf{p}}(t)$ $\hat{\mathbf{q}}_{k+1\|k} = \mathrm{e}^{\breve{\boldsymbol{\Omega}}_k T_s}\hat{\mathbf{q}}_{k\|k}$
Measurement prediction	begin {for $i = 1 : m$} $\overline{\mathbf{b}}^{(i)}_{k+1\|k} = \mathbf{D}(\hat{\mathbf{q}}_{k+1\|k})\mathbf{r}^{(i)}_{k+1}$ $\mathbf{P}^{b}_{k+1\|k} = \mathbf{H}^{(i)}_{\mathbf{p},k+1}\mathbf{P}^{\mathbf{p}}_{k+1\|k}\mathbf{H}^{(i)'}_{\mathbf{p},k+1} + \mathbf{R}^{(i)}_{b,k+1}$
Update	$\mathbf{K}^{(i)}_{k+1} = \mathbf{P}^{\mathbf{p}}_{k+1\|k}\mathbf{H}^{(i)'}_{\mathbf{p},k+1}(\mathbf{P}^{b}_{k+1\|k})^{-1}$ $\hat{\mathbf{p}}^{(i)}_{k+1\|k+1} = \hat{\mathbf{p}}^{(i-1)}_{k+1\|k} + \mathbf{K}^{(i)}_{k+1}\left(\mathbf{b}^{(i)}_{k+1} - \overline{\mathbf{b}}^{(i)}_{k+1\|k}\right)$ $\mathbf{P}^{\mathbf{p}}_{k+1\|k+1} = \mathbf{P}^{\mathbf{p}}_{k+1\|k} - \mathbf{K}^{(i)}_{k+1}\mathbf{P}^{b}_{k+1\|k}\mathbf{K}'_{k+1}$ end {for}
Attitude reset	$\hat{\mathbf{q}}_{k+1\|k+1} = \delta\mathbf{q}(\hat{\mathbf{p}}^{(m)}_{k+1\|k+1}) \otimes \hat{\mathbf{q}}_{k+1\|k}$

3.5 Comments

In this Chapter was presented a solution for the attitude determination problem previously defined in the Chapter 2. The solution was simply designed to work flow oriented in a block diagram as shown in Figure 3.1. The block 1 is concerned to the landmark detection and identification via image processing. The block 2 constructs the vector measurements pairs given the output of the block 1. And finally the block 3 estimates the attitude using vector measurements, given the output of the block 2. The idea is also to allow this framework to receive different algorithms in each block, respecting the inputs and outputs.

It is important to comment that the gain of the SMEKF has similar structure to the optimal KF gain. In order to exemplify, consider two vector measurements, $\mathcal{I} = \{1,2\}$, constantly in the camera FOV. Representing equation (3.35) for $\mathcal{I} = \{1,2\}$, it follows

that:

$$i = 1: \quad \hat{\mathbf{p}}^{(1)}_{k+1|k} = \hat{\mathbf{p}}_{k+1|k} + \mathbf{K}^{(1)}_{k+1}\left(\mathbf{b}^{(1)}_{k+1} - \overline{\mathbf{b}}^{(1)}_{k+1|k}\right), \tag{3.36}$$

$$i = 2: \quad \hat{\mathbf{p}}^{(2)}_{k+1|k} = \hat{\mathbf{p}}^{(1)}_{k+1|k} + \mathbf{K}^{(2)}_{k+1}\left(\mathbf{b}^{(2)}_{k+1} - \overline{\mathbf{b}}^{(2)}_{k+1|k}\right). \tag{3.37}$$

Substituting equation (3.36) in (3.37) results in the updated state, as follows:

$$\hat{\mathbf{p}}_{k+1|k+1} = \hat{\mathbf{p}}^{(2)}_{k+1|k} = \hat{\mathbf{p}}_{k+1|k} + \mathbf{K}^{(1)}_{k+1}\left(\mathbf{b}^{(1)}_{k+1} - \overline{\mathbf{b}}^{(1)}_{k+1|k}\right) + \mathbf{K}^{(2)}_{k+1}\left(\mathbf{b}^{(2)}_{k+1} - \overline{\mathbf{b}}^{(2)}_{k+1|k}\right). \tag{3.38}$$

Rewriting equation (3.38) in matrix notation, it follows that:

$$\hat{\mathbf{p}}_{k+1|k+1} = \hat{\mathbf{p}}_{k+1|k} + \begin{bmatrix} \mathbf{K}^{(1)}_{k+1} & \mathbf{K}^{(2)}_{k+1} \end{bmatrix} \left(\begin{bmatrix} \mathbf{b}^{(1)}_{k+1} \\ \mathbf{b}^{(2)}_{k+1} \end{bmatrix} - \begin{bmatrix} \overline{\mathbf{b}}^{(1)}_{k+1} \\ \overline{\mathbf{b}}^{(2)}_{k+1} \end{bmatrix} \right), \tag{3.39}$$

where $\begin{bmatrix} \mathbf{K}^{(1)}_{k+1} & \mathbf{K}^{(2)}_{k+1} \end{bmatrix} = \mathbf{K}_{k+1}$ is the Kalman gain, which is given by

$$\mathbf{K}_{k+1} = \mathbf{P}^{\mathbf{p}}_{k+1|k}\mathbf{H}'_{\mathbf{p},k+1}\left(\mathbf{H}_{\mathbf{p},k+1}\mathbf{P}^{\mathbf{p}}_{k+1|k}\mathbf{H}'_{\mathbf{p},k+1} + \mathbf{R}_{b,k+1}\right)^{-1}. \tag{3.40}$$

Rewriting equation (3.40) in terms of $\begin{bmatrix} \mathbf{K}^{(1)}_{k+1} & \mathbf{K}^{(2)}_{k+1} \end{bmatrix}$, it is possible to define the sequen-

tial gain as follows:

$$\begin{bmatrix} \mathbf{K}_{k+1}^{(1)} & \mathbf{K}_{k+1}^{(2)} \end{bmatrix} = \mathbf{P} \begin{bmatrix} \mathbf{H}^{(1)} \\ \mathbf{H}^{(2)} \end{bmatrix}' \left(\begin{bmatrix} \mathbf{H}^{(1)} \\ \mathbf{H}^{(2)} \end{bmatrix} \mathbf{P} \begin{bmatrix} \mathbf{H}^{(1)} \\ \mathbf{H}^{(2)} \end{bmatrix}' + \begin{bmatrix} \mathbf{R}^{(1)} & 0_{3\times3} \\ 0_{3\times3} & \mathbf{R}^{(2)} \end{bmatrix} \right)^{-1}, \tag{3.41}$$

where $\mathbf{H}^{(1)} = \mathbf{H}_{\mathbf{p},k+1}^{(1)}$, $\mathbf{H}^{(2)} = \mathbf{H}_{\mathbf{p},k+1}^{(2)}$,$\mathbf{R}^{(1)} = \mathbf{R}_{b,k+1}^{(1)}$, $\mathbf{R}^{(2)} = \mathbf{R}_{b,k+1}^{(2)}$ and $\mathbf{P} = \mathbf{P}_{k+1|k}^{\mathbf{p}}$. Expanding the matrix multiplication of equation (3.41) results in:

$$\begin{bmatrix} \mathbf{K}_{k+1}^{(1)} & \mathbf{K}_{k+1}^{(2)} \end{bmatrix} = \begin{bmatrix} \mathbf{P}\left(\mathbf{H}^{(1)}\right)' & \mathbf{P}\left(\mathbf{H}^{(2)}\right)' \end{bmatrix} \begin{bmatrix} \mathbf{H}^{(1)}\mathbf{P}\left(\mathbf{H}^{(1)}\right)' + \mathbf{R}^{(1)} & \mathbf{H}^{(1)}\mathbf{P}\left(\mathbf{H}^{(2)}\right)' \\ \mathbf{H}^{(2)}\mathbf{P}\left(\mathbf{H}^{(1)}\right)' & \mathbf{H}^{(2)}\mathbf{P}\left(\mathbf{H}^{(2)}\right)' + \mathbf{R}^{(2)} \end{bmatrix}^{-1} \tag{3.42}$$

The secondary diagonal of the inverse matrix in equation (3.42), which is assumed to be null in order to perform the sequential update, is given by $\mathbf{H}_{\mathbf{p},k+1}^{(2)}\mathbf{P}_{k+1|k}^{\mathbf{p}}\mathbf{H}_{\mathbf{p},k+1}^{(1)'} = \mathbf{H}_{\mathbf{p},k+1}^{(1)}\mathbf{P}_{k+1|k}^{\mathbf{p}}\mathbf{H}_{\mathbf{p},k+1}^{(2)'}$. The aforementioned assumption is valid, since $\mathbf{H}_{\mathbf{p},k+1}^{(2)}\mathbf{P}_{k+1|k}^{\mathbf{p}}\mathbf{H}_{\mathbf{p},k+1}^{(1)'} < \mathbf{R}_{b,k+1}^{(i)}$[2]. The Figure 3.4 shows the value of $\xi = \mathbf{H}_{\mathbf{p},k+1}^{(1)}\mathbf{P}_{k+1|k}^{\mathbf{p}}\mathbf{H}_{\mathbf{p},k+1}^{(2)'}$.

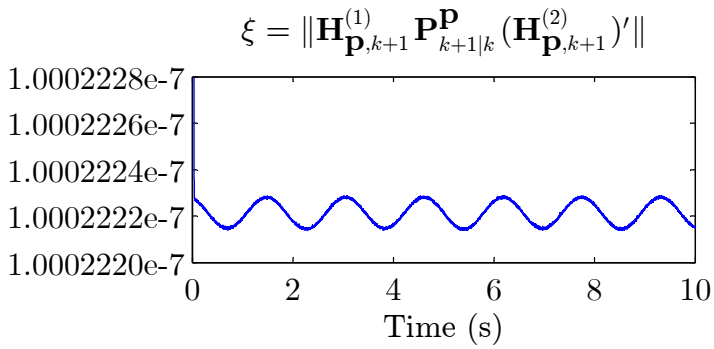

FIGURE 3.4 – The value of ξ during simulation.

[2]The value of $\mathbf{R}_b^{(i)}$ will be defined in Section 4.1, together with the other simulation parameters of Case 7.

4 Simulations and Results

The present section evaluates the SMEKF method. The evaluation is based on Monte Carlo simulations and shows the accuracy and convergence rate of the estimator. The Simulink 3D Animation environment is adopted in order to simulate the camera point of view and image processing steps of the method.

4.1 Simulation of the True Movement and Environment

In order to obtain data for the algorithm evaluation, the multirotor attitude dynamics is excited by the following sinusoidal angular velocities:

$$\boldsymbol{\omega}(t) = \begin{bmatrix} a\sin(f\mathrm{T_s k}) \\ a\cos(f\mathrm{T_s k}) \\ a\cos(f\mathrm{T_s k}) \end{bmatrix}, \tag{4.1}$$

where f and a are, respectively, a frequency and amplitudes parameters. The true attitude is computed by integrating equation (2.4) via Runge-Kutta 4 with fixed step of 0.001 seconds.

There are few references related to the flight maneuvers for validating AD systems in multirotor UAVs. In this manner, nine cases of angular velocities for the vehicle were defined in order to simulate different flight modes. Cases 1-3, 4-6 and 7-9, presented in Table 4.1, respectively define amplitudes and frequencies for hovering, slow flight and maximum inclination flight.

TABLE 4.1 – Simulated angular frequencies and amplitudes.

Case	f (rad/s)	a (rad/s)
1	2	$2\pi/180$
2	5	$2\pi/180$
3	10	$2\pi/180$
4	2	$6\pi/180$
5	5	$6\pi/180$
6	10	$6\pi/180$
7	2	$12\pi/180$
8	5	$12\pi/180$
9	10	$12\pi/180$

The uncertainty of the angular velocity is given by the zero-mean Gaussian white sequence $\{\delta\boldsymbol{\omega}_k\}$ with covariance $\mathbf{Q}_k$. Assuming that the camera lenses are not ideal, which results in image distortion and, consequently, vector measurement error, a zero-mean Gaussian white sequence $\{\delta\mathbf{b}_k^{(i)}\}$ with covariance $\mathbf{R}_{b,k}^{(i)}$ is added to the measurements. Both covariances $\mathbf{Q}_k$ and $\mathbf{R}_{b,k}^{(i)}$ were tuned by trial and error and are presented in Table 4.2. The values of both covariances are small when compared to low-cost sensors with available data-sheets in the internet.

TABLE 4.2 – Measurement noise covariances.

Sensor	Covariance
Rate-gyro	$\mathbf{Q}_k = (0.0005)^2\mathbf{I}_3$ (rad/s)^2
Camera	$\mathbf{R}_b^{(i)} = (0.001)^2\mathbf{I}_3$

The Simulink 3D Animation environment is illustrated in the Figure 4.1(a). The multirotor has been designed as a thin surface model and, consequently, does not have

mechanical properties. It is important to remember that the multirotor has fixed linear position and variable attitude. The vehicle is assumed to hover at position $[X_G \;\; Y_G \;\; Z_G]' = [0 \;\; 0 \;\; 1]'$, as illustrated in Figure 4.1(a).

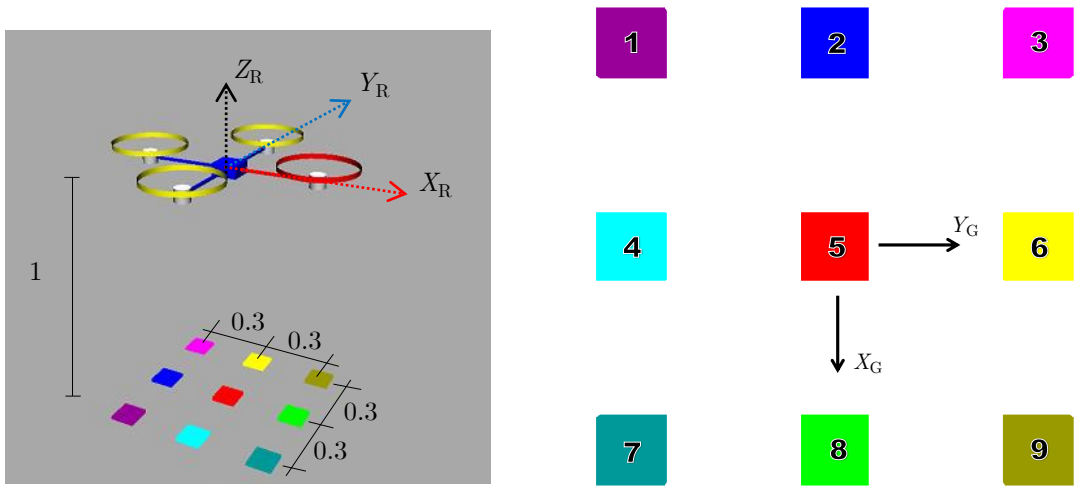

(a) (b)

FIGURE 4.1 – The simulation environment using Simulink 3D Animation and the camera point of view.

The map of the landmarks is shown in Figure 4.1(b) from the camera point of view. Table 4.3 shows the color of each landmark and theirs coordinates in the S_G system. The color of each landmark was chosen randomly.

TABLE 4.3 – The color and position of the landmarks.

Landmark	Color (R;G;B)	S_G Position (m)
1	(153;0;153)	(-0.3;-0.3;0)
2	(0;0;255)	(-0.3;0;0)
3	(255;0;255)	(-0.3;0.3;0)
4	(0;255;255)	(0;-0.3;0)
5	(255;0;0)	(0;0;0)
6	(255;255;0)	(0;0.3;0)
7	(0;153;153)	(0.3;-0.3;0)
8	(0;255;0)	(0.3;0;0)
9	(153;153;0)	(0.3;0.3;0)

4.2 Evaluation via Computational Simulation

The Sequential Multiplicative Extended Kalman Filter (SMEKF) is evaluated via Monte Carlo simulation with one hundred runs and using the simulated data obtained as described in Section 4.1. The initial conditions are represented in Euler angles (3-1-3) for better understanding. Before the simulation starts, the initial estimated attitude is converted to quaternion. The initialization error is assumed to have standard deviation equal to the maximum inclination during flight, which is twelve degrees. The initial estimation error covariance was tuned in order to minimize the convergence time via trial and error. Table 4.4 presents the adopted simulation parameters.

TABLE 4.4 – Simulation parameters.

Initial true attitude	$\mathbf{a}_0 = \begin{bmatrix} 0^o & 0^o & 0^o \end{bmatrix}'$
Initial estimated attitude	$\hat{\mathbf{q}}_0 \sim \text{a2q}\left[\mathcal{N}\left(\mathbf{a}_0, \mathbf{P}_0\right)\right]$
Initialization error covariance	$\mathbf{P}_0 = (12^o)^2 \mathbf{I}_3$
Initial estimated MRP	$\hat{\mathbf{p}}_{0\|0} = \begin{bmatrix} 0 & 0 & 0 \end{bmatrix}'$
Initial estimation error covariance	$\mathbf{P}^{\mathbf{p}}_{0\|0} = (0.5)^2 \mathbf{I}_3$
Sampling time	$\mathrm{T_s} = 0.001$ s
Monte Carlo realizations	MC = 100
Simulation time	T = 10 s
Camera frame rate	1/0.03 fps

The function a2q is adopted for converting the initial attitude from Euler angles to quaternions, which is given by equation (4.2) as follows (SHUSTER, 1993):

$$\text{a2q}(\mathbf{a}) = \begin{bmatrix} \cos\left(\dfrac{(\phi+\psi)}{2}\right)\cos\left(\dfrac{\theta}{2}\right) \\ \cos\left(\dfrac{(\phi-\psi)}{2}\right)\sin\left(\dfrac{\theta}{2}\right) \\ \sin\left(\dfrac{(\phi-\psi)}{2}\right)\sin\left(\dfrac{\theta}{2}\right) \\ \sin\left(\dfrac{(\phi+\psi)}{2}\right)\cos\left(\dfrac{\theta}{2}\right) \end{bmatrix}, \tag{4.2}$$

where ϕ, θ and ψ are the components of the Euler angle vector, as follows:

$$\mathbf{a} = \begin{bmatrix} \phi \\ \theta \\ \psi \end{bmatrix}. \tag{4.3}$$

In order to determine the accuracy of the filter, the following figure of merit is computed (SANTOS,):

$$\epsilon_k = \left| \mathrm{acos}\left(\frac{1}{2}\mathrm{tr}\left[\mathbf{D}(\mathbf{q}_{\mathrm{k}})\mathbf{D}(\hat{\mathbf{q}}_{\mathrm{k|k}})'\right] - \frac{1}{2} \right) \right|, \tag{4.4}$$

where ϵ_k corresponds to the attitude estimation error in the Euler principal angle notation. Note that ϵ_k has as property $\epsilon_k \geq 0$ and gets closer to zero as the estimated attitude approximates to the true attitude.

The horizontal acceleration of the vehicle is computed using the maximum $\bar{\epsilon}_k$. Assume the total thrust force of the multirotor, $u = 20$ N, to be collinear to Z_{B}, its mass to be $m = 1$ Kg and the attitude of the vehicle to be equal to the maximum attitude error $\bar{\epsilon}_k$ in the Euler principal angle notation. In order to compute the horizontal acceleration, it is necessary to decompose the total thrust force in the $X_{\mathrm{R}} - Y_{\mathrm{R}}$ plane, as illustrated in Figure 4.2. Given the previously defined parameters, one can compute the horizontal acceleration of the vehicle by the following equation:

$$a_h = \frac{u \sin(\bar{\epsilon}_k)}{m}. \tag{4.5}$$

For each simulated case, the equation (4.5) is computed. The Table 4.5 shows the results, including the acceleration of the vehicle in relation to the gravity.

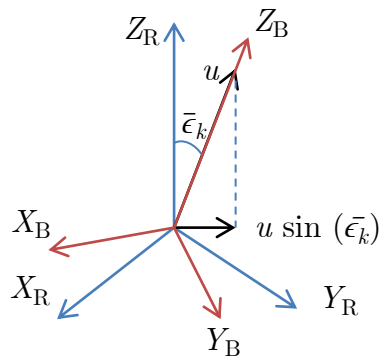

FIGURE 4.2 – Decomposition of the thrust force.

The goal is to evaluate the SMEKF based on one hundred samples of ϵ_k, from which is computed the sample mean $\bar{\epsilon}_k$ and the sample standard deviation $\sigma_{\epsilon,k}$ for each k instant. Figures 4.3, 4.4 and 4.5 show the computed mean, standard deviation and all realizations in the background. Table 4.5 shows the maximum values for $\bar{\epsilon}_k$ in the respective discrete time instant k.

The cases 1, 2 and 3 are shown in Figure 4.3. For case 1, the error frequency is approximated to $2\pi/3$ rad/s and the maximum error is 0.7366 degree. For case 2, the frequency of the error is $5\pi/3$ rad/s and the maximum error is 0.6229 degree. For case 3, the attitude error oscillates with frequency of approximately to $10\pi/3$ rad/s and the maximum error is 0.5694 degree. For $a = 2\pi/180$ rad/s, it is possible to conclude that the attitude error frequency is proportional to the frequency of the multirotor angular velocity by the factor of $\pi/3$.

The Figure 4.4 shows the cases 4, 5 and 6. For the case 4, the attitude error oscillates with frequency equal to $2\pi/3$ and the maximum error is 2 degree. The frequency of the attitude error in case 5 is $5\pi/3$ and the maximum error is 1.2640 degree. The attitude error frequency of case 6 is equal to $10\pi/3$ and the maximum error is 0.9059 degree. As

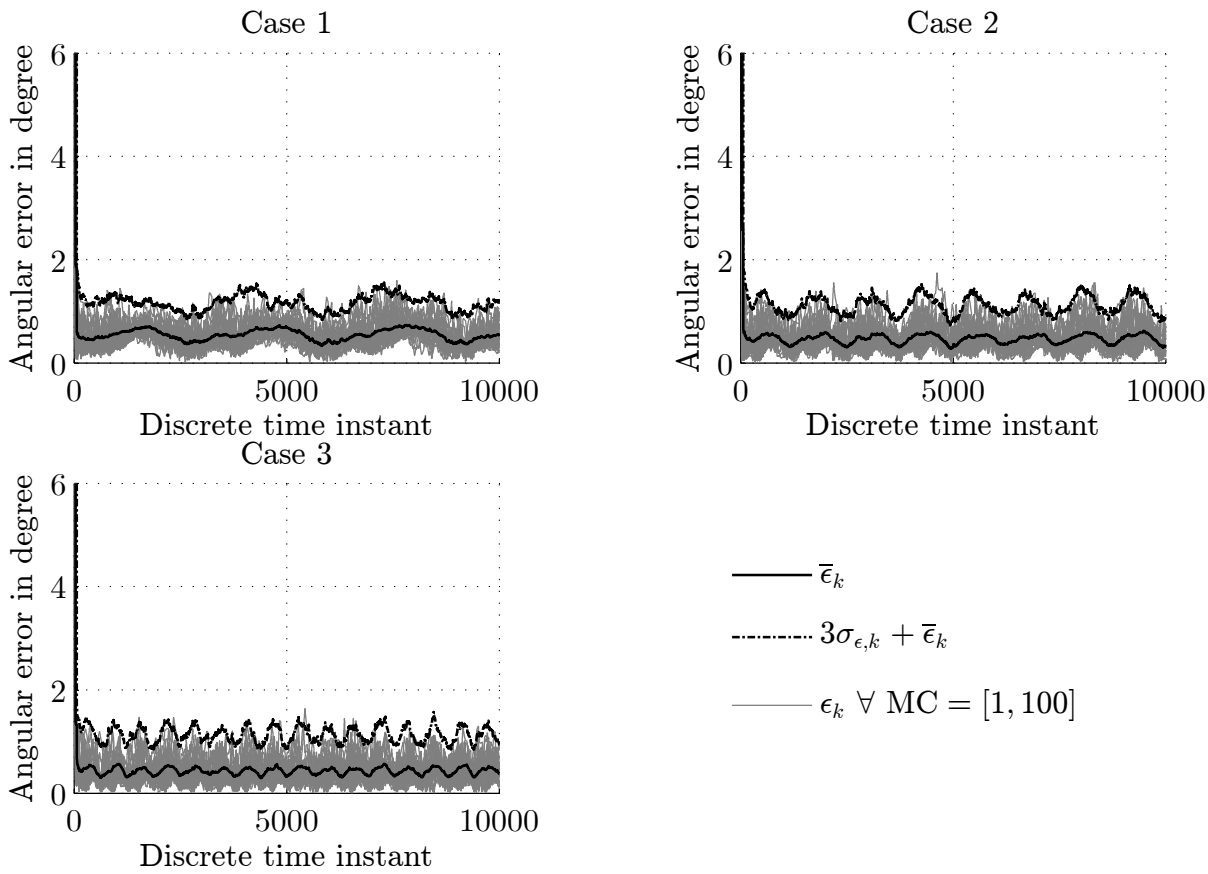

FIGURE 4.3 – Attitude error for cases 1-3.

well as cases 1-3, the cases 4-6 are related to the angular velocity frequency by the factor of $\pi/3$. However, note that the amplitude of the angular frequency increases by the factor of three. The growth in the amplitude caused the maximum error to increase in 59.09% for case 6 with respect to case 3, 102.92% for case 5 with respect to case 2, and 171.51% for case 4 with respect to case 1.

The Figure 4.5 shows the attitude error for cases 7, 8 and 9. The case 7 does not have a clear frequency and reaches 4.1570 degree in maximum error. For case 8, the frequency of the attitude error is approximated to $5\pi/3$ and the maximum error is 2.3730 degree. The attitude error at case 9 has frequency approximated to $10\pi/3$ and maximum error of 1.6470 degree. For cases 8 and 9, the frequencies of the attitude error are still proportional to the angular velocity frequency by the factor of $\pi/3$. Due to the growth in the angular

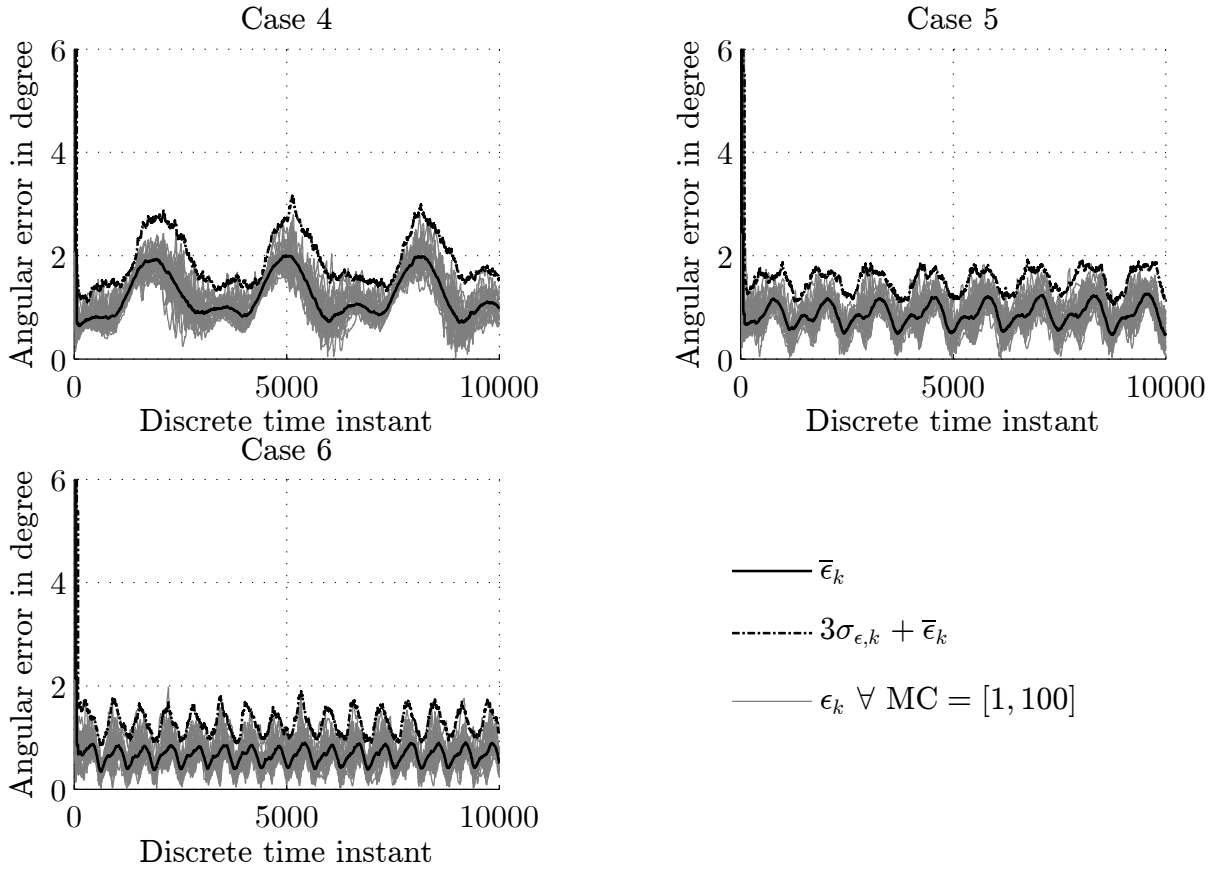

FIGURE 4.4 – Attitude error for cases 4-6.

velocity amplitude by the factor of two with respect to the last three cases, the attitude error increases by 81.80% from case 6 to case 9, 87.73% from case 5 to case 8, 107.85% from case 4 to case 7.

TABLE 4.5 – Attitude estimation results for the respective frequencies and amplitudes.

Case	f (rad/s)	a (rad/s)	Maximum $\overline{\epsilon}_k$	a_h (m/s^2)	a_h/g
1	2	$2\pi/180$	0.7366	0.2571	0.0262
2	5	$2\pi/180$	0.6229	0.2174	0.0221
3	10	$2\pi/180$	0.5694	0.1988	0.0202
4	2	$6\pi/180$	2.0000	0.6980	0.0711
5	5	$6\pi/180$	1.2640	0.4412	0.0449
6	10	$6\pi/180$	0.9059	0.3162	0.0322
7	2	$12\pi/180$	4.1570	1.4498	0.1477
8	5	$12\pi/180$	2.3730	0.8281	0.0844
9	10	$12\pi/180$	1.6470	0.5748	0.0585

The Figure 4.6 presents one typical run of of case 3 in Euler angles, which is the

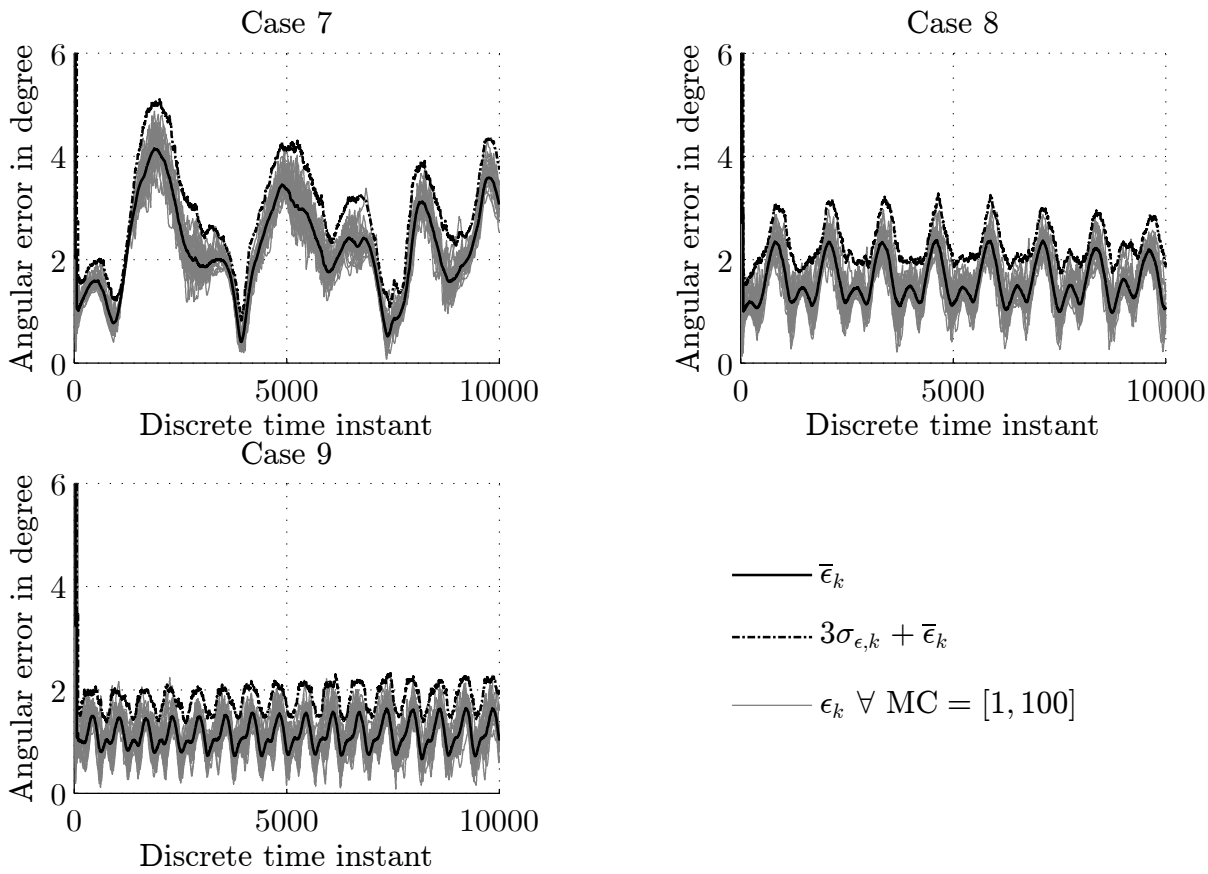

FIGURE 4.5 – Attitude error for cases 7-9.

best case simulated. It is possible to observe that the estimation error in the ψ angle is smaller than the others. This characteristic is due to the sensibility of the camera to small rotations around its own axis. On the other hand, the Figure 4.6 shows balanced estimation error in all Euler angles for a typical run of case 7, which is the worst case simulated.

Based on the results, it is possible to state that cases 4, 7, 8 and 9 present a considerable horizontal acceleration when compared to the gravity. On the other hand, cases 1, 2, 3, 5 and 6, present satisfactory results. The case 7 is the most critic due to the partial occlusion of the the landmarks from the camera field of view, which prevents the computation of its center of area.

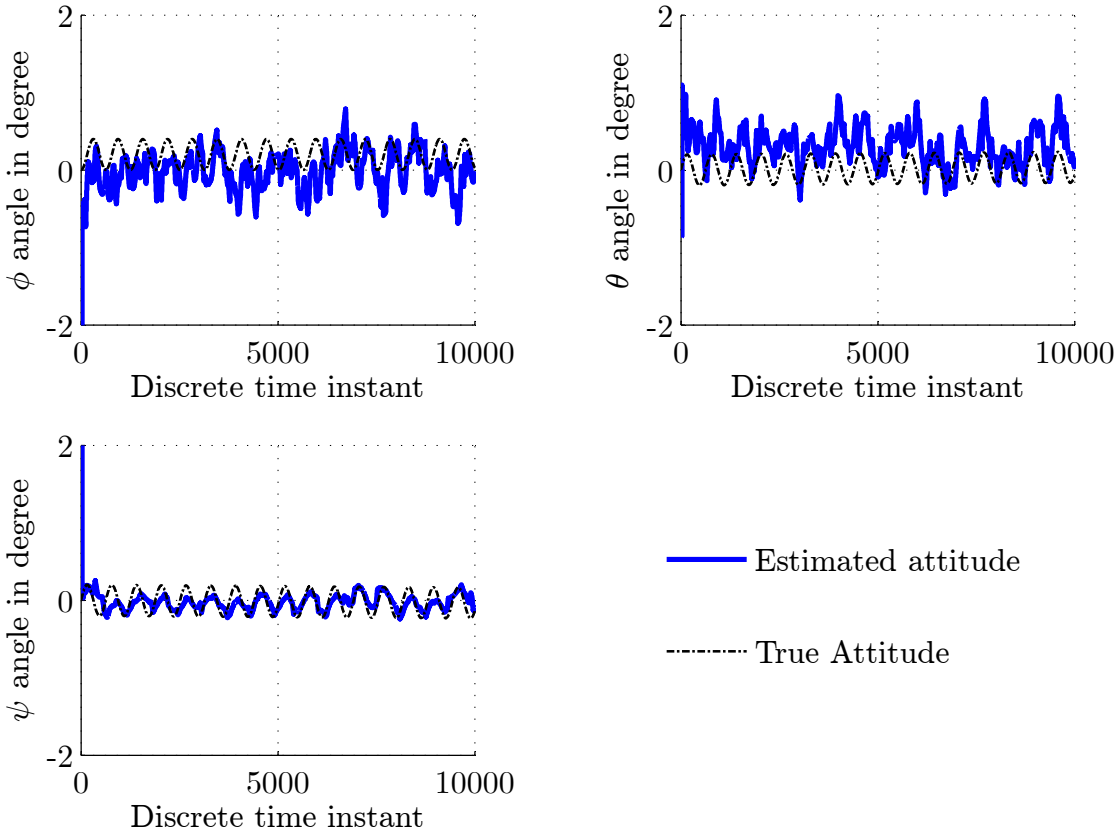

FIGURE 4.6 – Attitude in Euler angles for case 3.

4.3 Comments

It is notable the influence of both amplitude and frequency in the result of the attitude estimation. In particular, the movement becomes more critic as the frequency of the angular velocity decreases and its amplitude increases. This combination of high amplitude and low frequency results in a wide angular trajectory increasing the attitude estimation error, as seen in case 7. On the other hand, higher frequencies combined with low amplitudes, cause the filter to produce better results. These characteristics were expected since the minimum variance attitude estimation brings better results for more dynamic vector measurements. It is possible to conclude that the presented method is a good option for landing and coupling applications, since the expected angular velocities are compatible

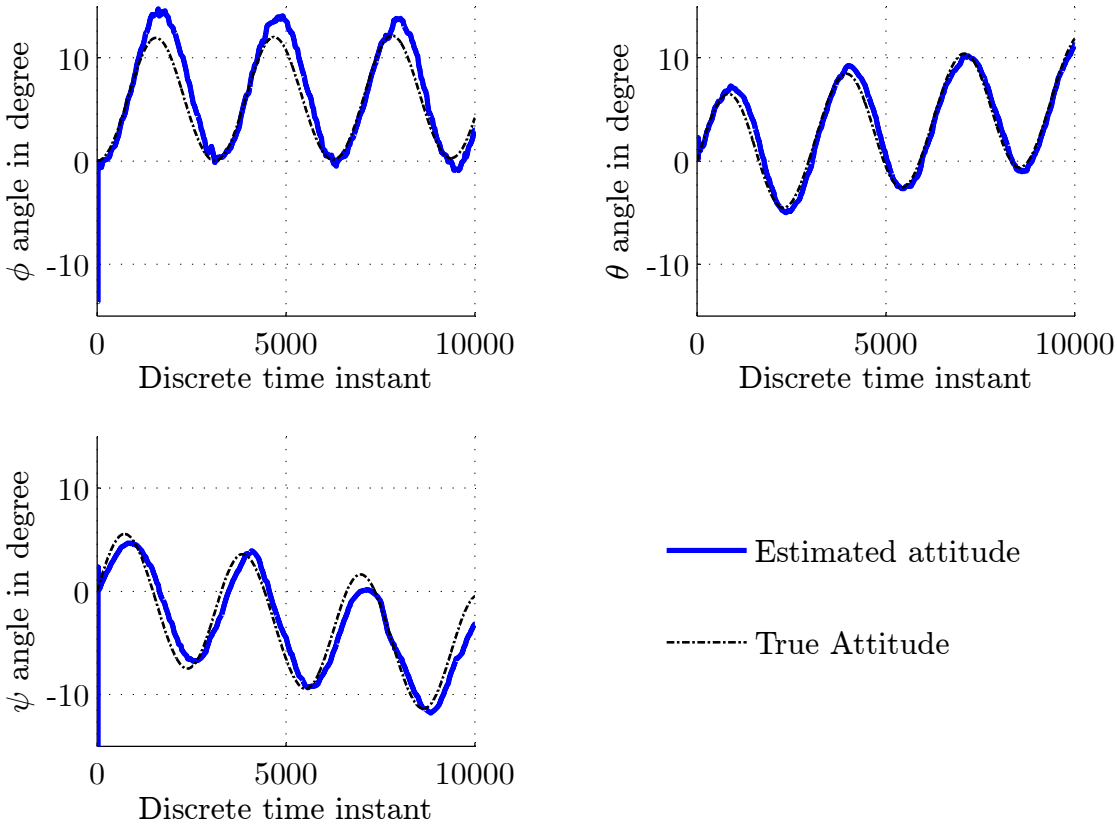

FIGURE 4.7 – Attitude in Euler angles for case 7.

with the characteristics of the best cases simulated.

5 Final Considerations

5.1 Conclusion

A complete solution for attitude determination, which uses pairs of vector measurements extracted from images, has been proposed in this work. It was motivated by the need of reliable vector measurements at indoor environments. Camera vector measurements can complement or even substitute measures susceptible to interference, such as the geomagnetic field vector.

The framework was presented in Chapter 3 as a modular method composed by three blocks. The image, which comes from the strapdown camera, is the main input and is processed in the first block. The algorithm of that phase was exposed in a didactic manner and left space for more complexes image processing methods. The second block is responsible for computing the vector measurement, and depends on the outcome from the first block. Finally, the sequential multiplicative extended Kalman filter (SMEKF) was proposed for the third block. As an advantage, the SMEKF is flexible with respect to the number of vector measurements, which decreased the dimension of the KF Jacobians.

The Chapter 4 proposed a three dimensional simulation environment in order to evaluate the proposed AD method. The Simulink 3D Animation environment allowed the

strapdown camera point of view, making the evaluation reliable and closer to the reality. As we were concerned only to the attitude determination, the multirotor only had angular movements. Nine different angular velocities were simulated in order to collect data for the evaluation. The performance index measures the angular error between the true and estimated attitudes in the Euler principal angle notation. It had been observed that lower frequencies combined with wider movements increases the estimation error.

Finally, this work adds a specific application for cameras, ensuring the high potential of its use in the aerial robotics field.

5.2 Future Work

The results of this work suggest a successful continuation of the research in this field. Some recommended researches that would complement this work are:

- Application of pattern recognition in the landmark identification step. This idea is a great upgrade in order to increase the flexibility of the attitude determination method. For example, shapes such as table corners, letters, numbers and different objects, could be used as landmarks for indoor navigation in the real world;

- Comparison between different attitude estimators such as the Quaternion Extended Kalman Filter (QEKF). In this case, a sequential version of the QEKF would depend on the additive update, making it difficult to maintain the quaternion norm;

- Analyze the application of other sensors such as accelerometer and magnetometer complementing the camera vector measurements.

References

BAR-ITZHACK, I. Y. Request - a recursive quest algorithm for sequential attitude determination. **Journal of Guidance, Control and Dynamics**, v. 19, p. 1034–1038, Oct. 1996.

BAR-ITZHACK, I. Y.; OSHMAN, Y. Attitude determination from vector observations: Quaternion estimation. **IEEE Transactions on Aerospace and Electronic Systems**, v. 21, p. 128–136, Jan. 1985.

BLOSCH, M. *et al.* Vision based MAV navigation in unknown and unstructured environments. In: IEEE INTERNATIONAL CONFERENCE ON ROBOTICS AND AUTOMATION, 2010, Anchorage. **Proceedings...**Piscataway: IEEE, 2010. p. 21–28.

CARRILLO, L. R. G. *et al.* Combining stereo vision and inertial navigation system for a quad-rotor UAV. **Journal of Intelligent and Robotic Systems**, v. 65, p. 373–387, Jan. 2012.

CHEVIRON, T. *et al.* Robust nonlinear fusion of inertial and visual data for position, velocity and attitude estimation of UAV. In: IEEE INTERNATIONAL CONFERENCE ON ROBOTICS AND AUTOMATION, 2007, Roma. **Proceedings...**Piscataway: IEEE, 2007. p. 2010–2016.

CHOUKROUN, D.; BAR-ITZHACK, I. Y.; OSHMAN, Y. Optimal-request algorithm for attitude determination. **Journal of Guidance, Control and Dynamics**, v. 27, p. 418–425, Jun. 2004.

ERGINER, B.; ALTUG, E. Modeling and pd control of a quadrotor vtol vehicle. In: IEEE INTELLIGENT VEHICLES SYMPOSIUM, 2007, Istanbul. **Proceedings...**Piscataway: IEEE, 2007. p. 894–899.

FARRELL, J. L. Attitude determination by Kalman filtering. **Automatica**, v. 6, p. 419–430, May 1970.

GEBRE-EGZIABHER, D.; ELKAIM, G. H. MAV attitude determination by vector matching. **IEEE Transactions on Aerospace and Electronic Systems**, v. 44, p. 1012–1028, Jul. 2008.

HOFFMANN, F.; GODDEMEIER, N.; BERTRAM, T. Attitude estimation and control of a quadrocopter. In: IEEE/RSJ INTERNATIONAL CONFERENCE ON INTELLIGENT ROBOTS AND SYSTEMS, 2010, Taipei. **Proceedings...**Piscataway: IEEE, 2010. p. 1072–1077.

HUANG, Y. *et al.* Development and prospect of unmanned aerial vehicle technologies for agricultural production management. **International Journal of Agricultural and Biological Engineering**, v. 6, p. 1–10, Sep. 2013.

IDAN, M. Estimation of rodrigues parameters from vector observations. **IEEE Transactions on Aerospace and Electronic Systems**, v. 32, p. 578–586, Apr. 1996.

KENDOUL, F.; YU, Z.; NONAMI, K. Guidance and nonlinear control system for autonomous flight of minirotorcraft unmanned aerial vehicles. **Journal of Field Robotics**, v. 27, p. 311–334, Jun 2010.

KIM, C.; KIM, T.; LYOU, J. Realization of a mems attitude reference system for a small aerial vehicle. In: IEEE ANNUAL CONFERENCE ON INDUSTRIAL ELECTRONICS, 38., 2012, Montreal. **Proceedings...**Piscataway: IEEE, 2012. p. 1567–1570.

KLEIN, G.; MURRAY, D. Parallel tracking and mapping for small AR workspaces. In: IEEE AND ACM INTERNATIONAL SYMPOSIUM ON MIXED AND AUGMENTED REALITY, 6., 2007, Nara. **Proceedings...**Piscataway: IEEE, 2007.

LEFFERTS, E. J.; MARKLEY, F. L.; SHUSTER, M. D. Kalman filtering for spacecraft attitude estimation. **Journal of Guidance, Control and Dynamics**, v. 5, p. 417–429, Jan 1982.

MANCINI, F. *et al.* Using unmanned aerial vehicles (UAV) for high-resolution reconstruction of topography: The structure from motion approach on coastal environments. **Remote Sensing**, v. 5, p. 6880–6898, Dec 2013.

MARKLEY, F. L. Attitude error representations for Kalman filtering. **Journal of Guidance, Control, and Dynamics**, v. 26, p. 311–317, Apr 2003.

MARKLEY, F. L.; CRASSIDIS, J. L. Attitude estimation using modified rodrigues parameters. In: FLIGHT MECHANICS/ESTIMATION THEORY SYMPOSIUM, 1996, Greenbelt. **Proceedings...**Washington, DC: NASA, 1996. p. 71–83.

OLTMANNS, S. O. *et al.* Unmanned aerial vehicle (UAV) for monitoring soil erosion in morocco. **Remote Sensing**, v. 4, p. 3390–3416, Nov 2012.

SANTOS, D. A. **Estimação de atitude e velocidade angular de satélites utilizando medidas do campo geomagnético e da direção do Sol.** 2008. 156 f. Dissertação (Mestrado em Sistemas e Controle) — Engenharia Eletrônica e Computação, Instituto Tecnológico de Aeronáutica, São José dos Campos.

SANTOS, D. A.; SAOTOME, O.; CELA, A. **Position formation control of multirotor helicopters with thrust vector constraints.** In: IEEE MEDITERRANEAN CONFERENCE ON CONTROL AND AUTOMATION, 21th., 2013, Platanias-Chania. **Proceedings...**Piscataway: IEEE, 2013.

SCHAUB, H. **Novel coordinates for nonlinear multibody motion with applications to spacecraft dynamics and control.** 1998. Tese (PhD) — Aerospace Engineering, Texas A M University, College Station.

SHABAYEK, A. E. R. *et al.* Vision based UAV attitude estimation: Progress and insights. **Journal of Intelligent and Robotic Systems**, v. 65, p. 295–308, Jan 2012.

SHUSTER, M. D. A survey of attitude representations. **Journal of the Astronautical Sciences**, v. 41, p. 439–517, Dec 1993.

SHUSTER, M. D.; OH, S. D. Three-axis attitude determination from vector observations. **Journal of Guidance, Control and Dynamics**, v. 4, p. 70–77, Feb 1981.

TARHAN, M.; ALTUG, E. EKF based attitude estimation and stabilization of a quadrotor UAV using vanishing points in catadioptric images. **Journal of Intelligent and Robotic Systems**, v. 62, p. 587–607, Jun. 2011.

TAYYAB, M. *et al.* Design of a blimp based unmanned aerial vehicle for surveillance. **International Journal of Engineering and Technology**, v. 5, p. 519–530, Mar. 2013.

TOURNIER, G. P. *et al.* Estimation and control of a quadrotor vehicle using monocular vision and moire patterns. In: AIAA GUIDANCE, NAVIGATION, AND CONTROL CONFERENCE AND EXHIBIT, 2006, Keystone. **Proceedings...**Washington, DC: AIAA, 2006. p. 21–24.

WANG, S.; YANG, Y. Quadrotor aircraft attitude estimation and control based on Kalman filter. In: CHINESE CONTROL CONFERENCE, 31., 2012, Hefei. **Proceedings...**Piscataway: IEEE, 2012. p. 5634–5639.

WERTZ, J. R. (Ed.). **Spacecraft Attitude Determination and control**. Dordrecht: Kluwer Academic Publ., 1978. (Astrophysics and space science library, v.73).

ZHAN, Q.; WANG, J.; XI, X. Control system design and experiments of a quadrotor. In: INTERNATIONAL CONFERENCE ON ROBOTICS AND BIOMIMETICS, 2012, Guangzhou. **Proceedings...**Piscataway: IEEE, 2012. p. 1152–1157.

Appendix A - Attitude Determination Algorithm

This appendix presents the attitude determination algorithm divided according to Chapter 3. The results presented in Chapter 4 were obtained using the present algorithm, implemented in MATLAB/Simulink R2012b. The Figure A.1 shows the Simulink diagram used in this work.

A.1 Algorithm of the Block 1: Detection and Identification of Landmarks

```
function [J,l] = class(I,ID)

% Inputs:
%       I: Captured Image;
%       ID: Landmark Colors.
% Outputs:
%       J: Black & White Image;
%       l: Landmark position.

[i,j,p] = size(I);
J = ones(i,j);

% The variable Color Identified (CID) stores the position of the
```

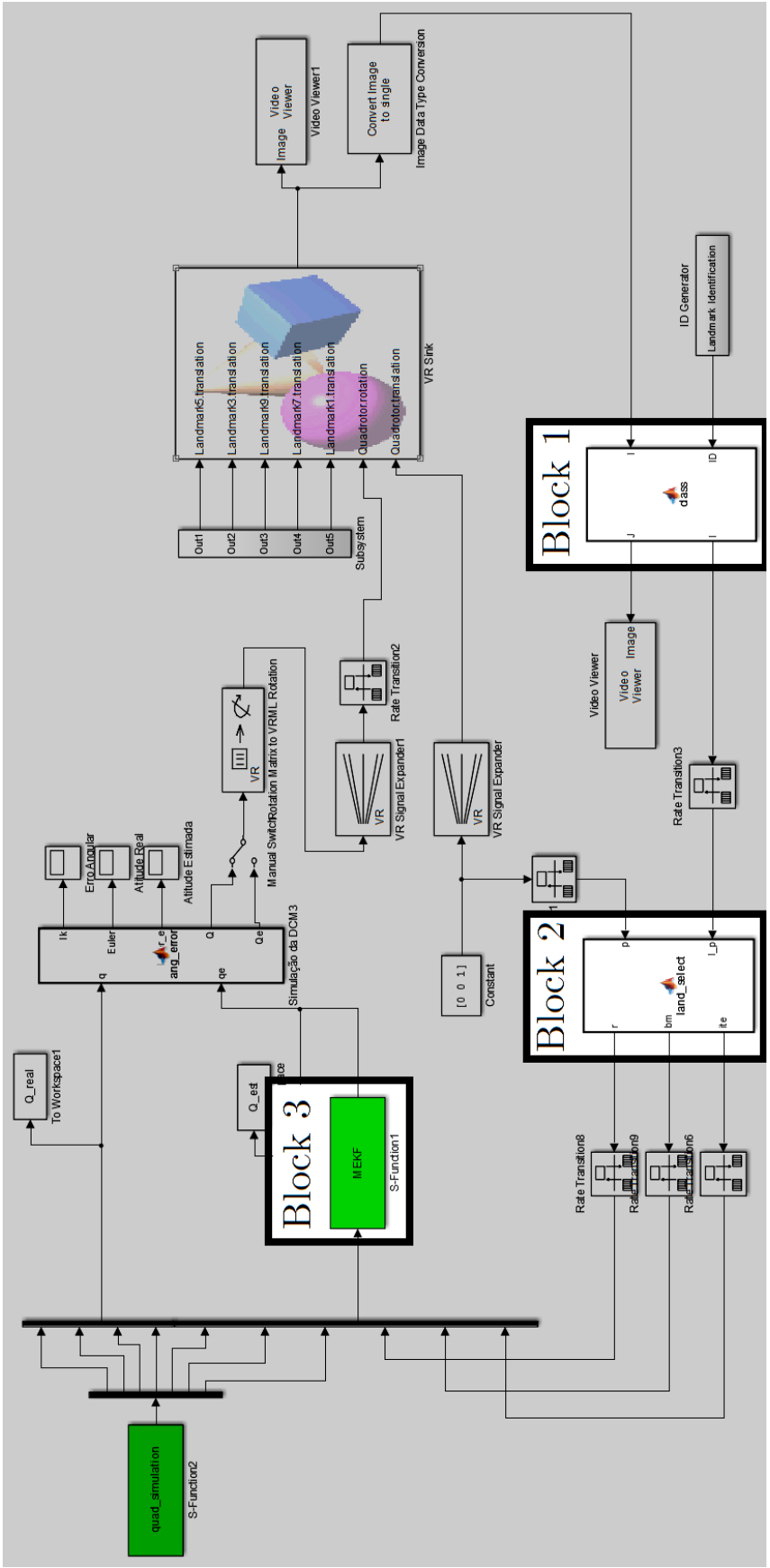

FIGURE A.1 – The diagram of the simulated method in Simulink.

```
% first and last pixels detected. Before each loop, the position
% is assumed to be out of the image.

CID1 = ones(2,2)*400;
i1=1;
CID2 = ones(2,2)*400;
i2=1;
CID3 = ones(2,2)*400;
i3=1;
CID4 = ones(2,2)*400;
i4=1;
CID5 = ones(2,2)*400;
i5=1;
CID6 = ones(2,2)*400;
i6=1;
CID7 = ones(2,2)*400;
i7=1;
CID8 = ones(2,2)*400;
i8=1;
CID9 = ones(2,2)*400;
i9=1;

% The variables tr, tg and tb measures the sensibility of the
% color identification. For the current simulation, the
% comparison between the identified color and the stored color is
% equal to zero.

tr=0.0;
tg=0.0;
tb=0.0;

% The matrix A stores the difference between the identified color
% and the stored color.

A = zeros(3,9);
Ml = ID;
for L=1:i
        for C=1:j
            if I(L,C,1)==I(L,C,2)&&I(L,C,3)==I(L,C,2)
                J(L,C)=1;
            else
                Mi = [I(L,C,1) I(L,C,2) I(L,C,3)]'/256;
                A(:,1)=abs(Mi-Ml(:,1));
                A(:,2)=abs(Mi-Ml(:,2));
                A(:,3)=abs(Mi-Ml(:,3));
                A(:,4)=abs(Mi-Ml(:,4));
                A(:,5)=abs(Mi-Ml(:,5));
```

```
                A(:,6)=abs(Mi-Ml(:,6));
                A(:,7)=abs(Mi-Ml(:,7));
                A(:,8)=abs(Mi-Ml(:,8));
                A(:,9)=abs(Mi-Ml(:,9));
                if (A(1,1))≤tr && (A(2,1))≤tg && (A(3,1))≤tb
                    if i1==1
                        CID1(:,i1)=[L;C];
                        i1=2;
                    end
                    CID1(:,i1)=[L;C];
                    J(L,C)=0;
                elseif (A(1,2))^2≤tr&&(A(2,2))^2≤tg&&(A(3,2))^2≤tb
                    if i2==1
                        CID2(:,i2)=[L;C];
                        i2=2;
                    end
                    CID2(:,i2)=[L;C];
                    J(L,C)=0;
                elseif (A(1,3))^2≤tr&&(A(2,3))^2≤tg&&(A(3,3))^2≤tb
                    if i3==1
                        CID3(:,i3)=[L;C];
                        i3=2;
                    end
                    CID3(:,i3)=[L;C];
                    J(L,C)=0;
                elseif (A(1,4))^2≤tr&&(A(2,4))^2≤tg&&(A(3,4))^2≤tb
                    if i4==1
                        CID4(:,i4)=[L;C];
                        i4=2;
                    end
                    CID4(:,i4)=[L;C];
                    J(L,C)=0;
                elseif (A(1,5))^2≤tr&&(A(2,5))^2≤tg&&(A(3,5))^2≤tb
                    if i5==1
                        CID5(:,i5)=[L;C];
                        i5=2;
                    end
                    CID5(:,i5)=[L;C];
                    J(L,C)=0;
                elseif (A(1,6))^2≤tr&&(A(2,6))^2≤tg&&(A(3,6))^2≤tb
                    if i6==1
                        CID6(:,i6)=[L;C];
                        i6=2;
                    end
                    CID6(:,i6)=[L;C];
                    J(L,C)=0;
                elseif (A(1,7))^2≤tr&&(A(2,7))^2≤tg&&(A(3,7))^2≤tb
```

```
                    if i7==1
                        CID7(:,i7)=[L;C];
                        i7=2;
                    end
                    CID7(:,i7)=[L;C];
                    J(L,C)=0;
                elseif (A(1,8))^2≤tr&&(A(2,8))^2≤tg&&(A(3,8))^2≤tb
                    if i8==1
                        CID8(:,i8)=[L;C];
                        i8=2;
                    end
                    CID8(:,i8)=[L;C];
                    J(L,C)=0;
                elseif (A(1,9))^2≤tr&&(A(2,9))^2≤tg&&(A(3,9))^2≤tb
                    if i9==1
                        CID9(:,i9)=[L;C];
                        i9=2;
                    end
                    CID9(:,i9)=[L;C];
                    J(L,C)=0;
                end
            end
        end
end

% The calculation of the center of the landmark is developed
% below:

l1 = CID1(:,1)+floor((CID1(:,2)-CID1(:,1))/2);
l2 = CID2(:,1)+floor((CID2(:,2)-CID2(:,1))/2);
l3 = CID3(:,1)+floor((CID3(:,2)-CID3(:,1))/2);
l4 = CID4(:,1)+floor((CID4(:,2)-CID4(:,1))/2);
l5 = CID5(:,1)+floor((CID5(:,2)-CID5(:,1))/2);
l6 = CID6(:,1)+floor((CID6(:,2)-CID6(:,1))/2);
l7 = CID7(:,1)+floor((CID7(:,2)-CID7(:,1))/2);
l8 = CID8(:,1)+floor((CID8(:,2)-CID8(:,1))/2);
l9 = CID9(:,1)+floor((CID9(:,2)-CID9(:,1))/2);

% The center of the Cartesian Coordinate System is transferred to
% the center of the image in the following:

l1 = l1-[i;j]*.5;
l2 = l2-[i;j]*.5;
l3 = l3-[i;j]*.5;
l4 = l4-[i;j]*.5;
l5 = l5-[i;j]*.5;
l6 = l6-[i;j]*.5;
```

```
l7 = l7-[i;j]*.5;
l8 = l8-[i;j]*.5;
l9 = l9-[i;j]*.5;

l=[l1 l2 l3 l4 l5 l6 l7 l8 l9];

end
```

A.2 Algorithm of the Block 2: Construction of Vector Measurements

```
function [r,bm,ite] = land_select(p,l_p)

% Inputs:
%       p: Position of the multirotor in the Ground CCS;
%       l_p: Landmark position in the Image CCS.
% Outputs:
%       r: Vector measurement in the Reference CCS;
%       bm: Vector measurement in the Body CCS;
%       ite: Flag for the number of iterations in the SMEKF.

% Position of the landmarks in the Ground CCS:

d1_r = [-0.3;-0.3;0];
d2_r = [-0.3;0;0];
d3_r = [-0.3;0.3;0];
d4_r = [0;-0.3;0];
d5_r = [0;0;0];
d6_r = [0;0.3;0];
d7_r = [0.3;-0.3;0];
d8_r = [0.3;0;0];
d9_r = [0.3;0.3;0];

% Computation of the vector measurements in the Reference CCS:

l_r = [(d1_r-p)/norm(d1_r-p) (d2_r-p)/norm(d2_r-p) ...
    (d3_r-p)/norm(d3_r-p)...
     (d4_r-p)/norm(d4_r-p) (d5_r-p)/norm(d5_r-p) (d6_r-p)/norm(d6_r-p)...
     (d7_r-p)/norm(d7_r-p) (d8_r-p)/norm(d8_r-p) (d9_r-p)/norm(d9_r-p)];
r = [l_r(:,1)' l_r(:,3)' l_r(:,5)' l_r(:,7)' l_r(:,9)']';

% Computation of the vector measurements in the Body CCS:

l = [l_p(:,1) l_p(:,3) l_p(:,5) l_p(:,7) l_p(:,9)];
a = length(l);
ite = zeros(1,a);
z = ones(a,1)*-p(3);
alpha = zeros(a,1);
cbeta = zeros(a,1);
sbeta = zeros(a,1);
n_l = ones(a,1);
l_x = l(1,:);
```

```
l_b = [l; z'];
k = 1/120; % Relation between distance, in meters, and pixels:
    for i=1:a
        if abs(l_x(i))<81
            n_l(i) = norm(l(:,i));
            alpha(i) = asin((n_l(i))*k);
            if n_l(i)==0
                cbeta(i) = 0;
                sbeta(i) = 0;
            else
                cbeta(i) = l(1,i)/n_l(i);
                sbeta(i) = l(2,i)/n_l(i);
            end
            l_b(:,i)=[sin(alpha(i))*cbeta(i) sin(alpha(i))*sbeta(i) ...
                -cos(alpha(i))]';
            ite(i) = 1;
        else
            ite(i) = 0;
        end
    end
bm = [l_b(:,1)' l_b(:,2)' l_b(:,3)' l_b(:,4)' l_b(:,5)']';
end
```

A.3 Algorithm of the Block 3: Attitude Estimation from Vector Measurements

```
% Inputs:
%       w: Angular velocity;
%       r: Vector measurement in the Reference CCS;
%       bm: Vector measurement in the Body CCS;
%       ite: Flag for the number of iterations in the SMEKF.
% Outputs:
%       qek: Estimated attitude quaternion.

    w = u(1:3);
    r(:,1) = u(4:6);
    r(:,2) = u(7:9);
    r(:,3) = u(10:12);
    r(:,4) = u(13:15);
    r(:,5) = u(16:18);
    bm(:,1) = u(19:21);
    bm(:,2) = u(22:24);
    bm(:,3) = u(25:27);
    bm(:,4) = u(28:30);
    bm(:,5) = u(31:33);
    ite = u(34:38);
    Pm(1:3,1) = x(1:3);
    Pm(1:3,2) = x(4:6);
    Pm(1:3,3) = x(7:9);
    qek = x(10:13);
    l = length(ite);

% State propagation

    w_x = [0      -w(3)   w(2);
           w(3)    0     -w(1);
          -w(2)    w(1)   0];
    Fm = (1/2)*-w_x;
    Pmk1 = Pm+(Fm*Pm+Pm*Fm'+Qm)*dt;
    W = 0.5*[0 -w'; w -w_x];
    n_w = norm(w);
    fi = cos(n_w*dt/2)*eye(4) + 1/n_w*sin(n_w*dt/2)*W;
    qek1 = fi*qek;
    qek1 = qek1/norm(qek1);
    qe_x = [0 -qek1(4) qek1(3); qek1(4) 0 -qek1(2); -qek1(3) qek1(2) 0];
    De = (qek1(1)^2-qek1(2:4)'*qek1(2:4))*eye(3)+ ...
        2*qek1(2:4)*qek1(2:4)'-2*qek1(1)*qe_x;
```

```
    pk1=[0 0 0]';
    b = zeros(3,l);

% Measurement prediction

    for i=1:l
       if ite(i)==1
           r_x = [0       -r(3,i)   r(2,i);
                  r(3,i)   0       -r(1,i);
                 -r(2,i)   r(1,i)   0];
           pk1_x = [0       -pk1(3)   pk1(2);
                    pk1(3)   0       -pk1(1);
                   -pk1(2)   pk1(1)   0];
           b(:,i) = De*r(:,i);
           b_x = [0       -b(3,i)   b(2,i);
                  b(3,i)   0       -b(1,i);
                 -b(2,i)   b(1,i)   0];
           Hm = (4/(1+pk1'*pk1)^2)*b_x*((1-pk1'*pk1)*eye(3) ...
               -2*pk1_x+2*(pk1*pk1'));
           Pmbk1 = Pmk1*Hm';

% Update

           K = Pmbk1/Pbk1;
           pk1 = pk1+K*(bm(:,i)-b(:,i)-Hm*pk1);
           Pmk1 = Pmk1-K*Pbk1*K';
       end
    end
    n_p = (norm(pk1))^2;
    dqk1(1) = (1-n_p)/(1+n_p);
    dqk1(2) = 2*pk1(1)/(1+n_p);
    dqk1(3) = 2*pk1(2)/(1+n_p);
    dqk1(4) = 2*pk1(3)/(1+n_p);

% Attitude reset

    qek1(1) = ...
        qek1(1)*dqk1(1)-qek1(2)*dqk1(2)-qek1(3)*dqk1(3)-qek1(4)*dqk1(4);
    qek1(2) = ...
        qek1(1)*dqk1(2)+qek1(2)*dqk1(1)-qek1(3)*dqk1(4)+qek1(4)*dqk1(3);
    qek1(3) = ...
        qek1(1)*dqk1(3)+qek1(2)*dqk1(4)+qek1(3)*dqk1(1)-qek1(4)*dqk1(2);
    qek1(4) = ...
        qek1(1)*dqk1(4)-qek1(2)*dqk1(3)+qek1(3)*dqk1(2)+qek1(4)*dqk1(1);
```

FOLHA DE REGISTRO DO DOCUMENTO

1. CLASSIFICAÇÃO/TIPO	2. DATA	3. REGISTRO N°	4. N° DE PÁGINAS
DM	06 de janeiro de 2015	DCTA/ITA/DM-082/2014	70

5. TÍTULO E SUBTÍTULO:

Attitude determination of a multirotor aerial vehicle using camera vector measurements and gyros.

6. AUTOR(ES):

Pedro Filizola Sousa Maia Gonçalves

7. INSTITUIÇÃO(ÕES)/ÓRGÃO(S) INTERNO(S)/DIVISÃO(ÕES):

Instituto Tecnológico de Aeronáutica – ITA

8. PALAVRAS-CHAVE SUGERIDAS PELO AUTOR:

Aerial robotics, Kalman filter, Attitude determination, Computer vision.

9.PALAVRAS-CHAVE RESULTANTES DE INDEXAÇÃO:

Aeronave não-tripulada; Filtros de Kalman; Estimação de estado; Giroscópios; Câmeras; Navegação aérea; Engenharia aeronáutica.

10. APRESENTAÇÃO: **(X) Nacional** **( ) Internacional**

ITA, São José dos Campos. Curso de Mestrado. Programa de Pós-Graduação em Engenharia Aeronáutica e Mecânica. Área de Sistemas Aeroespaciais e Mecatrônica. Orientador: Davi Antônio dos Santos. Defesa em 18/12/2014. Publicada em 2014.

11. RESUMO:

The employment of embedded cameras in navigation and guidance of Unmanned Aerial Vehicles (UAV) has attracted the focus of many academic researches. In particular, for the multirotor UAV, the camera is widely employed for applications performed at indoor environments, where are less access to the GNSS signal and higher electromagnetic interference. Nevertheless, in most researches, the images captured by the camera are usually adopted to aid in the linear position/velocity estimation, but not specifically for assisting in the attitude determination process. This dissertation proposes an attitude determination method for multirotor UAVs using pairs of vector measurements taken from one downward facing strapdown camera and angular velocity measurements from gyros. The method consists in three modules. The first detects and identifies landmarks from the captured images. The second module computes the vector measurements related to the direction between the landmarks and the camera. The third module executes the attitude estimation from the vector measurements given by the second module. The employed estimation method consists in a version of the Multiplicative Extended Kalman Filter (MEKF) with sequential update. The proposed method was evaluated via Monte Carlo simulations using Simulink 3D Animation. During the evaluation, the method presented effectiveness and satisfactory results in most of the simulated cases. Finally, future works are suggested for the potential continuation of this research.

12. GRAU DE SIGILO:

(X) OSTENSIVO **( ) RESERVADO** **( ) CONFIDENCIAL** **( ) SECRETO**